SIEMENS

Imaging Life

The Magazine for Molecular Imaging Innovation

Issue 09 | Clinical Case Supplement

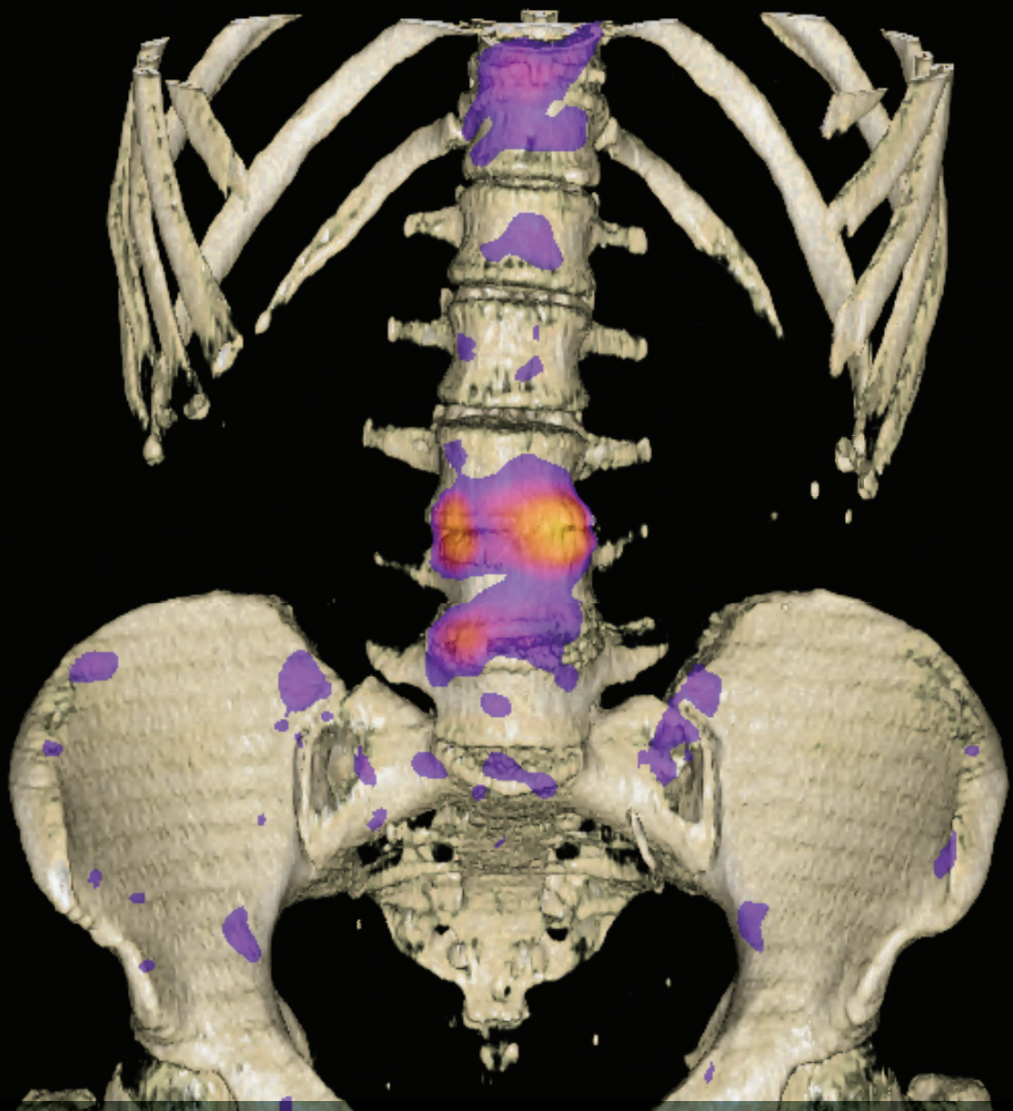

Delineation of Severe Osteochondrosis with xSPECT Bone

Page 22

Sharper Delineation of Small Pulmonary Metastases with HD•Chest in a Patient with Breast Carcinoma

Page 04

SPECT•CT for Patient-specific Dosimetry in Radionuclide Therapy

Page 34

Table of Contents

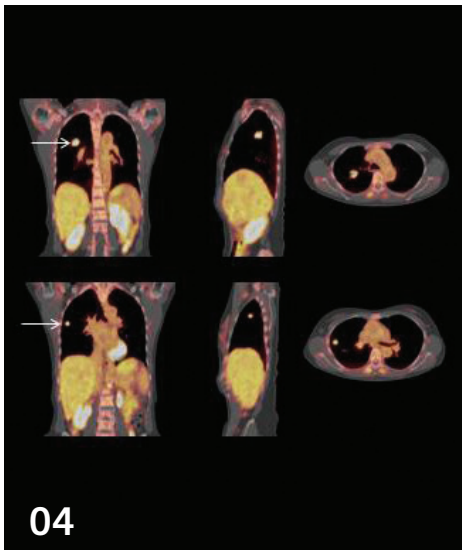

04

Sharper Delineation of Small Pulmonary Metastases with HD•Chest in a Patient with Breast Carcinoma

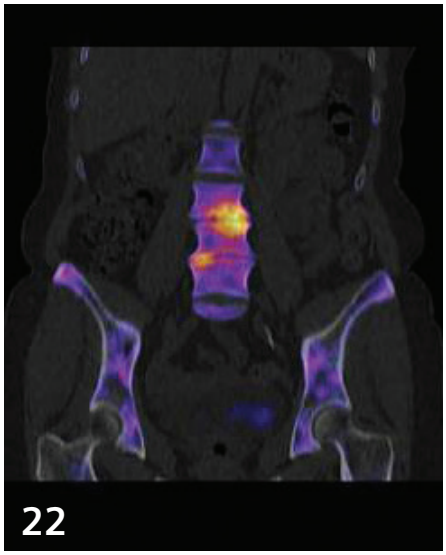

22

Delineation of Severe Osteochondrosis with xSPECT Bone

Imaging Life

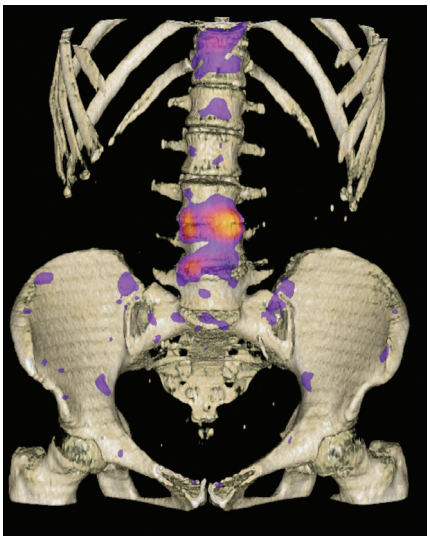

Clinical Case Studies

04 Sharper Delineation of Small Pulmonary Metastases with HD•Chest in a Patient with Breast Carcinoma

06 Improved Visualization of Focal Lymphomatous Deposit in Gastric Wall using ^{18}F FDG PET•CT and HD•Chest

08 Detection of Brain Metastases in a Patient Operated Neuroendocrine Tumor with Ga-68 DOTATATE PET•CT

10 Extension of Radiation Field Based on PET•CT in a Patient with Anal Carcinoma

12 Choline PET•CT Detection of Metastases in a Patient with Primary Prostate Carcinoma

14 Evaluation of Response to Radiation Therapy (IMRT) using Choline PET•CT in a Patient with Metastatic Prostate Carcinoma

18 Improved Characterization of Ischial Tendinitis using xSPECT Bone

22 Delineation of Severe Osteochondrosis with xSPECT Bone

24 Femoral Osteoid Osteoma Delineated by ^{99m}Tc MDP xSPECT Bone

26 Reversible Anteroseptal Ischemia Detected by Stress-rest Myocardial Perfusion using IQ•SPECT

30 Pre-operative Assessment of Lung Perfusion using ^{99m}Tc MAA SPECT•CT in a Case of Epidermal Naevus Syndrome with Hemi-Dysplasia

Science

34 SPECT•CT for Patient-specific Dosimetry in Radionuclide Therapy

36 Subscription

37 Imprint

38 Prescribing Information

Sharper Delineation of Small Pulmonary Metastases with HD•Chest in a Patient with Breast Carcinoma

By **Dustin Osborne, PhD**

Data courtesy of the University of Tennessee Medical Center, Knoxville, TN, USA

History

A 65-year-old woman with a history of breast carcinoma was initially treated with lumpectomy and local radiation therapy. With evidence of a lung nodule from a chest X-ray, the patient presented for a follow-up. Due to the possibility of metastases, the patient was referred for Fludeoxyglucose F-18 (^{18}F FDG)* PET•CT.

An ^{18}F FDG PET•CT study was performed 90 minutes following an IV injection of 11 mCi of ^{18}F FDG. Variable table speed FlowMotion™ acquisition was performed on a Biograph mCT Flow™** system with incorporation of respiratory gating in the region comprising of the lungs and the upper part of the liver. This was acquired with a slow table speed (0.5 mm/sec) with integrated respiratory gating for this extended range. The region of the head and neck was scanned at a standard table speed (1 mm/sec), while the pelvis and extremities were scanned with faster table speeds (1.5 mm/sec) for optimized acquisition time. The gated thoracic and abdominal regions were reconstructed with HD•Chest for motion-frozen images and improved lesion detectability. Whole-body, non-gated images at 200x200 matrix were also reconstructed from the variable table speed acquisition. (The table speeds and ranges are demonstrated in *Figure 1*.)

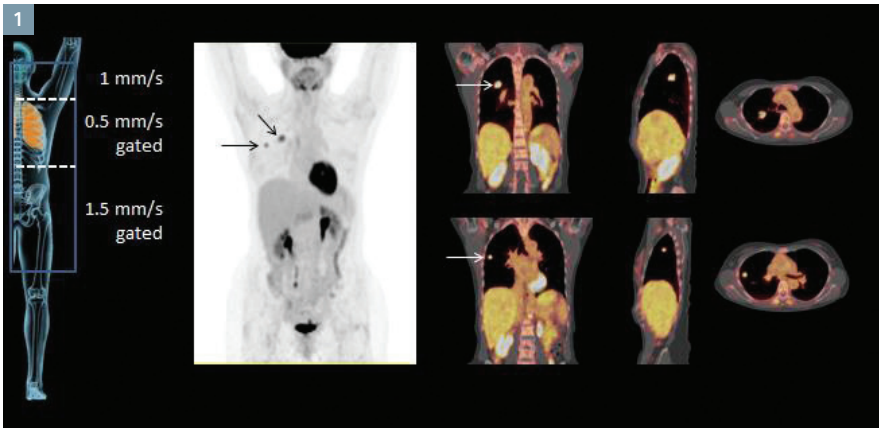

1 Whole-body PET•CT study demonstrates 2 hypermetabolic lung nodules.

Diagnosis

Figure 1 shows a non-gated 200x200 matrix reconstruction of the whole-body PET•CT that was acquired with variable table speeds. Two hypermetabolic metastatic lung nodules were visualized in the right upper lobe. No other distant metastases were visualized.

The HD•Chest images, reconstructed with 33% of the gated list mode data and with low respiratory motion, showed, in comparison to non-gated PET, sharper delineation and higher lesion-to-background contrast of a small 8 mm hypermetabolic lung nodule (*Figure 2, arrows*), due to elimination of respiratory motion-related blurring by HD•Chest. In the non-gated reconstruction, this small nodule was not well visualized in the PET MIP images (*Figure 1*) and was poorly delineated with low ^{18}F FDG uptake in the fused PET•CT images and the PET MPR slices (*Figure 2*).

Comments

Improved visualization of such small lesions with motion management—provided by respiratory gating and HD•Chest reconstruction—increases diagnostic confidence in the detection of lung metastases in cancers such as breast, bladder, thyroid and colorectal tumors. In this particular clinical case, improved detection of additional small lung metastases did not necessarily result in a major change in the therapy decision due to the presence of two larger lung metastases. In such situations, aggressive chemotherapy is generally the therapy of choice, since ablation of individual lung metastases is ruled out because of the presence of multiple lesions. Improved localization of a small right, lower-lung-base metastasis did however highlight the disseminated spread of microscopic metastases and the potential for appearance of new lesions. Aggressive chemotherapy also aims to reduce the metastatic burden and slow the appearance of new lesions, which is

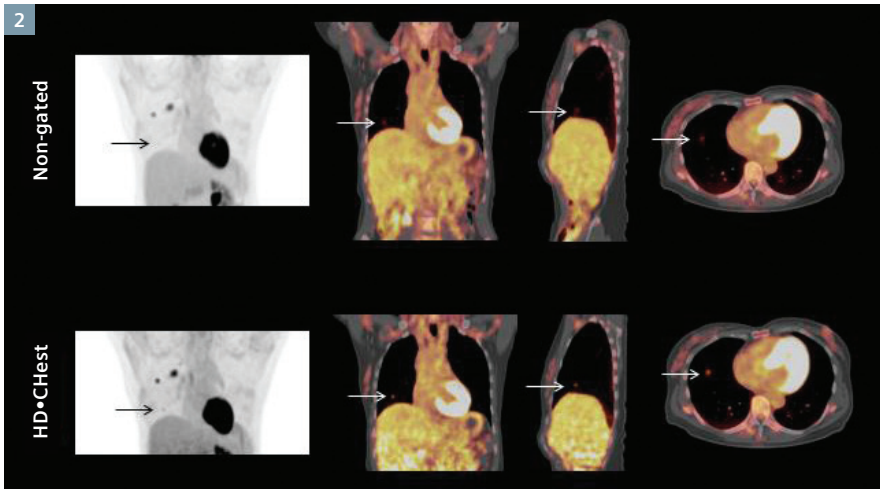

2 Comparison of MIP and fused PET•CT images of HD•Chest and non-gated reconstructions of the thorax shows improved delineation of a small nodular metastatic lesion in the lower-right lung with HD•Chest (*arrow*).

also advantageous in this case. Since chemotherapy is associated with systemic effects, and ablation of solitary or multiple small lung or liver lesions is a therapy option, improved lesion detectability offered by HD•Chest motion management is helpful for patient management decisions.

Conclusion

Flexible range of respiratory gating, made possible with variable table speed FlowMotion acquisition, imparts the ability to perform gating on limited or extended regions without undue time penalty. HD•Chest reconstructions obtained from gated list mode data provide relatively motion-frozen images. This improves the detectability and SUV quantification of small lesions subject to significant respiratory motion and related blurring as well as partial volume effects, as demonstrated in this clinical example.

Examination Protocol

Scanner	Biograph mCT Flow 64
Injected Dose	11 mCi ^{18}F FDG
Scan Delay	90 min post injection
Acquisition	Zone 1, 1 mm/sec; Zone 2, 0.5 mm/sec gated; Zone 3, 1.5 mm/sec
CT	Whole-body scan mode; tube voltage, 120 kV; tube current, 152 eff mAs; slice collimation, 64x0.6 mm; slice thickness, 5 mm; CTDIvol, 11.63 mGy

* Indications and important safety information on Fludeoxyglucose F 18 injection can be found below. The full prescribing information can be found on pages 38-40.

** Biograph mCT Flow is not commercially available in all countries. Due to regulatory reasons its future availability cannot be guaranteed. Please contact your local Siemens organization for further details.

The statements by Siemens customers described herein are based on results that were achieved in the customer's unique setting. Since there is no "typical" hospital and many variables exists (e.g., hospital size, case mix, level of IT adoption) there can be no guarantee that other customers will achieve the same results.

Fludeoxyglucose F18 5-10mCi as an IV injection

Indications and Usage

Fludeoxyglucose F 18 Injection (^{18}F FDG) is indicated for positron emission tomography (PET) imaging in the following settings:

- **Oncology:** For assessment of abnormal glucose metabolism to assist in the evaluation of malignancy in patients with known or suspected abnormalities found by other testing modalities, or in patients with an existing diagnosis of cancer.

Important Safety Information

- **Radiation Risks:** Radiation-emitting products, including Fludeoxyglucose F 18 Injection, may increase the risk for cancer, especially in pediatric patients. Use the smallest dose necessary for imaging and ensure safe handling to protect the patient and health care worker.
- **Blood Glucose Abnormalities:** In the oncology and neurology setting, suboptimal imaging may occur in patients with inadequately regulated blood glucose levels. In these patients, consider medical therapy and laboratory testing to assure at least two days of normoglycemia prior to Fludeoxyglucose F 18 Injection administration.
- **Adverse Reactions:** Hypersensitivity reactions with pruritus, edema and rash have been reported; have emergency resuscitation equipment and personnel immediately available.

Full prescribing information for Fludeoxyglucose F 18 Injection can be found on page 38-40.

Fludeoxyglucose F 18 injection is manufactured by Siemens' PETNET Solutions, 810 Innovation Drive, Knoxville, TN 39732

Improved Visualization of Focal Lymphomatous Deposit in Gastric Wall using ^{18}F FDG* PET•CT and HD•Chest

By **Dustin Osborne, PhD**

Data courtesy of the University of Tennessee Medical Center, Knoxville, TN, USA

History

A 55-year-old man with a long-standing history of gastritis presented with a single episode of profuse vomiting that contained blood stains. A gastric endoscopy demonstrated an area of thickening of rugae and inflammation in the mucosa of the gastric fundus. A histopathology from the biopsy sample from that mucosal segment showed gastric mucosa-associated lymphoid tissue (MALT) lymphoma. The patient was referred for a Fludeoxyglucose F-18 (^{18}F FDG) PET•CT to evaluate the extent of the tumor as well as extra gastric spread or other nodal involvement.

The study was performed on a Biograph mCT Flow™** system using continuous-bed-motion (FlowMotion™) acquisition, a technique that enables flexible range acquisitions with variable table speeds and, depending on the organ or region of interest, the ability to incorporate respiratory gating for any range. Because respiratory motion can affect the gastric lesional uptake and the perigastric region, a respiratory-gated acquisition was performed on the thorax and abdomen as part of the FlowMotion acquisition. Amplitude-based gated images were obtained with HD•Chest, using 33% of the list mode respiratory-gated data to obtain relatively motion-frozen images for improved delineation of lesions subjected to respiratory motion-induced blurring.

Diagnosis

HD•Chest images showed a small focal area of increased uptake in the gastric mucosa at the region of the gastric fundus (*Figure 1*, *cross-hairs*). The non-gated images did not show significantly higher uptake within the lesion when compared to the rest of the gastric mucosa. However, the HD•Chest images showed higher lesion contrast with the elimination of respiratory motion-related blurring. This makes visualization of the small solitary gastric lesion possible. There were no other hypermetabolic lesions in the gastric mucosa, the perigastric region or the loco-regional lymph nodes, suggesting that the patient had a small solitary MALT gastric lymphoma with an indolent course and good prognosis.

Comments

Although MALT lymphomas are uncommon, they frequently involve the stomach mucosa. ^{18}F FDG PET/CT has shown lower detection rates for MALT lymphomas in the stomach (62%) when compared to those in the bronchus (94%) or the head and neck (90%).[1] Although MALT lymphomas are ^{18}F FDG avid, the lower sensitivity of PET/CT for gastric lymphoma may be related to a smaller initial size, lower uptake and motion. Elimination of respiratory motion using HD•Chest improves detection of small gastric lesions as in the present case.

The standard uptake value (SUV) of MALT lymphomas have shown to correlate significantly with pathological malignant potentials, with high-grade MALT lymphomas demonstrating higher SUV.[2] Since HD•Chest improves the accuracy of SUV calculation in a small lesion by eliminating respiratory motion-related blurring, this technique can improve characterization of such lesions and help differentiate low grade indolent lesions from more aggressive ones. SUV_{max} has helped differentiate gastric MALT lymphomas from gastric carcinoma, which demonstrated higher values, although both conditions show similar gastrointestinal wall thickness on CT.[3] A high SUV in the baseline ^{18}F FDG PET/CT, and a lower reduction in the SUV within three months after H.Pylori eradication therapy, has shown to be associated with treatment-failure in

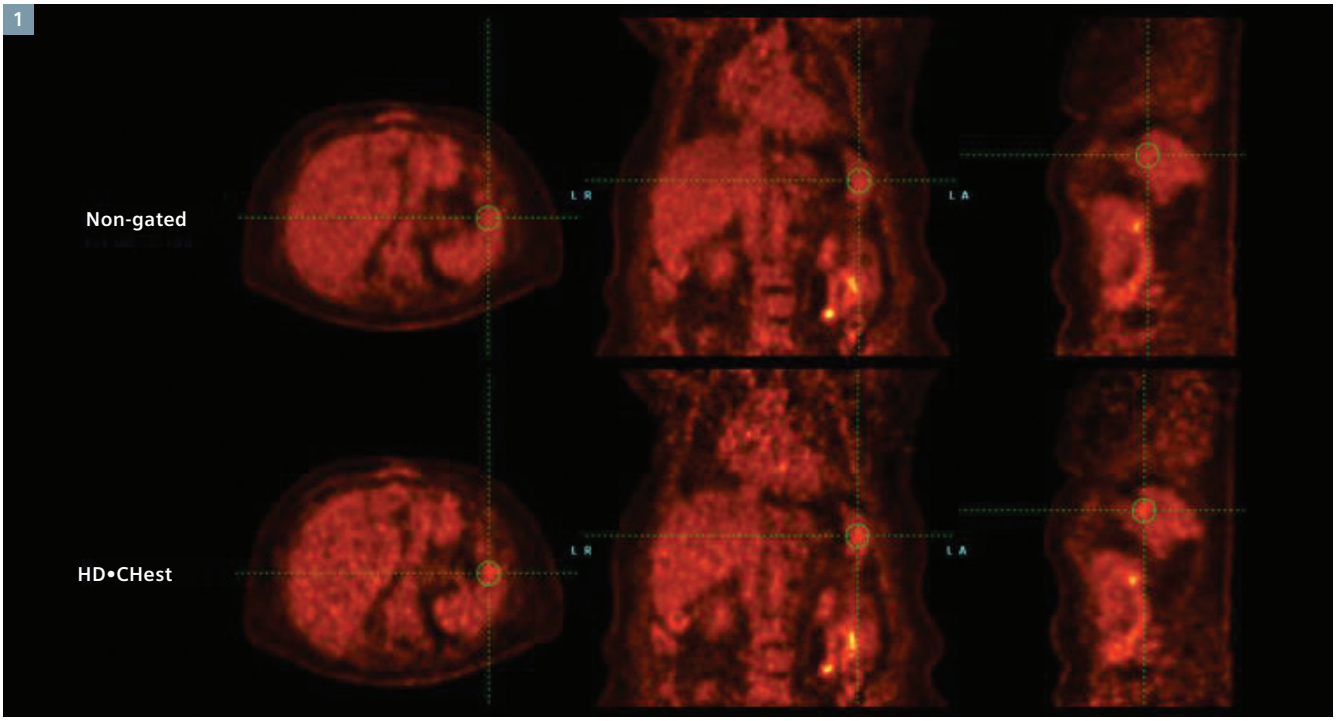

1 Comparison of non-gated PET and HD•Chest images of the thorax and upper abdomen demonstrates improved visualization of the small focal area of increased uptake in the gastric mucosa.

H.Pylori-positive, low-grade gastric MALT lymphoma patients who are undergoing eradication treatment.[4] These studies indicate the importance of SUV accuracy and higher detectability for initial staging, characterization, prognostication and therapy follow-up.

Conclusion

HD•Chest helps improve lesion detectability by eliminating respiratory motion-related blurring and quantitative accuracy of SUV. Integration of respiratory gating and HD•Chest in flexible ranges, which is made possible by FlowMotion acquisition, provides a seamless workflow and can be used routinely in patient imaging. As a result, a large range of patients, especially those with suspected liver, gastric or pancreatic lesions, could receive improved accuracy in PET imaging.

Examination Protocol

Scanner	Biograph mCT Flow 64
Injected Dose	11 mCi of ^{18}F FDG
Scan Delay	90 min post injection
CT	Whole-body scan mode; tube voltage, 120 kV; tube current, 141 eff mAs; slice collimation, 64x0.6 mm; slice thickness, 5 mm

References:
1. **Treglia et al.** *Hematol Oncol.* 2014.
2. **Watanabe et al.** *Int. J. Hematol.* 2013. 97(1): 43-49.
3. **Fu et al.** *PLoS ONE.* 2012. 7(12): e50914.
4. **Song et al.** *Gut Liver.* 2011; 5: 308-31.

* Indications and important safety information on Fludeoxyglucose F 18 injection can be found on page 05. The full prescribing information can be found on pages 38-40.

** Biograph mCT Flow is not commercially available in all countries. Due to regulatory reasons its future availability cannot be guaranteed. Please contact your local Siemens organization for further details.

The statements by Siemens customers described herein are based on results that were achieved in the customer's unique setting. Since there is no "typical" hospital and many variables exists (e.g., hospital size, case mix, level of IT adoption) there can be no guarantee that other customers will achieve the same results.

Detection of Brain Metastases in a Patient Operated Neuroendocrine Tumor with Ga-68 DOTATATE* PET•CT

By **Frank Bengel, MD**

Data courtesy of Medical University of Hannover, Hannover, Germany

History

A 59-year-old man with a history of a high-grade neuroendocrine tumor (carcinoid) in the intestine with metastases in the right lobe of the liver, who had been treated with intestinal resection and right hemihepatectomy, presented with rising serum chromogranin A levels. This was suspicious for tumor recurrence. As such, the patient was referred for Ga-68 DOTATATE PET•CT for the detection of a potential recurrent neuroendocrine tumor.

The PET•CT study was performed 1 hour after an intravenous injection of 150 MBq of Ga-68 DOTATATE. The study was performed on a Biograph mCT Flow™**, using continuous-bed-motion (FlowMotion™) acquisition and a uniform table speed of 0.7 mm/sec following a low-dose CT for attenuation correction. A whole-body PET•CT study was reconstructed with a standard matrix of 200x200. The brain was separately reconstructed with a higher matrix of 400x400, in order to obtain a sharper definition of cerebral lesions.

Diagnosis

Ga-68 DOTATATE PET•CT showed multiple focal areas of increased uptake in the brain, which suggested cerebral metastases (*Figure 1*). There were no other well-defined focal lesions in the body that suggested metastases. The remaining part of the liver (left lobe, post right hemihepatectomy status) was enlarged

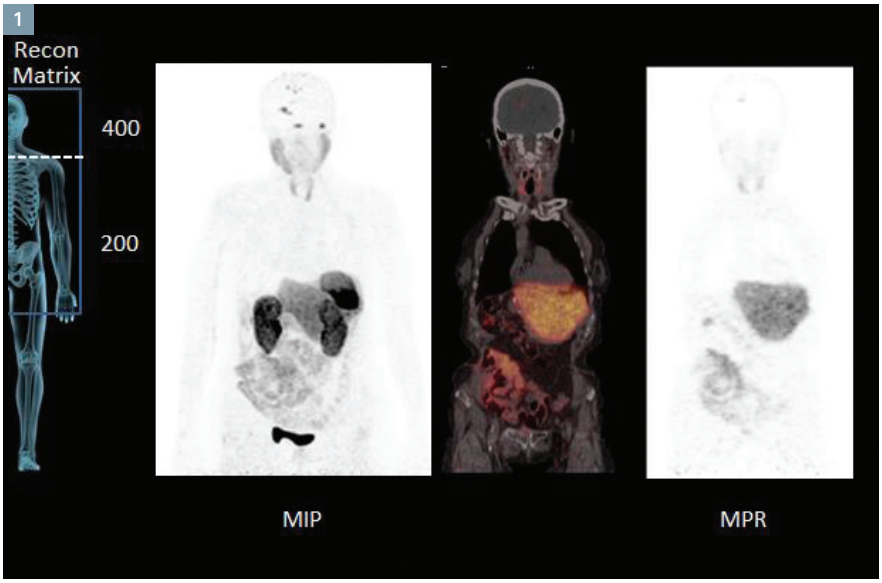

1 Whole-body 200x200 matrix reconstructions of Ga-68 DOTATATE PET•CT and fused images show multiple focal uptakes in the brain, which suggested metastases.

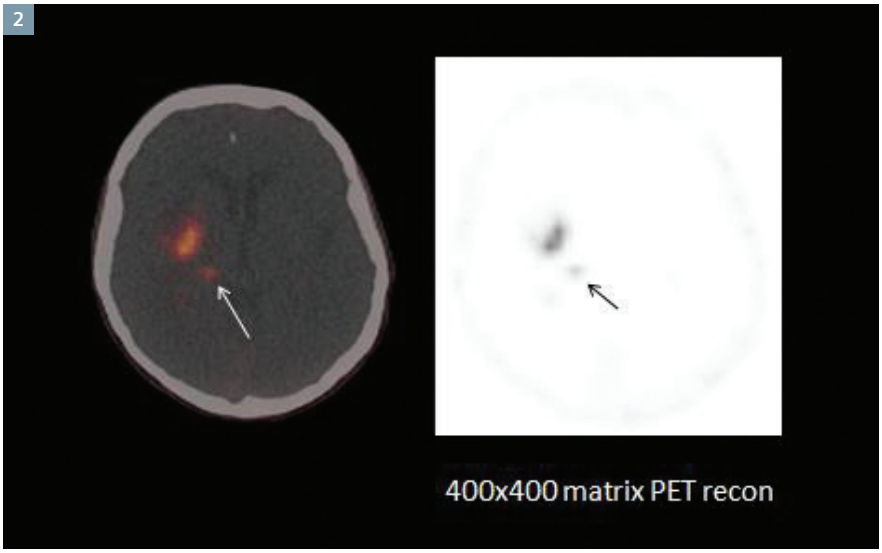

2 Hi-Rez 400x400 matrix PET reconstruction of the brain and fused images show multiple focal areas of tracer uptake in the right parietal cortex and basal ganglial region.

secondary to hypertrophy as expected, with uniform and normal tracer uptake. The spleen, kidneys, salivary glands and thyroid showed normal tracer uptake, as per the physiological distribution of Ga-68 DOTATATE. There was a considerable amount of tracer uptake in the small bowel, but without any focal abnormal area of uptake.

400x400 matrix reconstructions of Ga-68 DOTATATE PET•CT (*Figure 2*) showed multiple focal areas of increased uptake in the brain parenchyma, which suggested functioning neuroendocrine tumor metastases. Hi-Rez PET reconstructions delineated small brain metastases (*arrows*) due to a lower partial volume effect. High count statistics obtained by a slower continuous-bed-motion acquisition with a bed travel speed of 0.7 mm/sec were the key to achieving high image quality and lesion contrast, even with a higher matrix reconstruction with a smaller voxel size.

Because functioning brain metastases were detected with avid Ga-68 DOTATATE uptake, peptide receptor radionuclide therapy (PRRT) with Lu-177 DOTATATE* was considered as part of the approach for managing the metastatic brain lesions.

Comments

PET/CT using Ga-68-labelleled somatostatin analogs has been used in neuroendocrine tumors that overexpress somatostatin receptors. Approximately half of patients have metastatic disease at presentation, and early, accurate diagnosis and staging are crucial for therapy decisions. One of the main advantages of PET/CT is the possibility of quantifying tracer uptake, which reflects receptor density of the tumor and thus facilitates personalized diagnosis and therapy.

Similar to Ga-68 DOTATOC or DOTATATE, PET/CT with Ga-68 somatostatin analogs has demonstrated high impact on patient management in several studies. These studies have shown that a course of treatment had changed in 50%-60% of cases because of PET/CT results.[1] A meta-analysis of 16 clinical studies, involving 567 patients with suspected thoracic or gastroenteropancreatic NETs,[2] found pooled sensitivity and specificity of PET/CT with Ga-68 somatostatin analogs to be 93% and 91%, respectively, for detection of primary or metastatic NET. In such patients, the analysis recommends that Ga-68 somatostatin analogs be considered as a first-line diagnostic imaging method. Analogs like Ga-68 DOTATOC, Ga-68 DOTATATE and Ga-68 DOTANOC are extensively used in clinical studies demonstrating fast pharmacokinetics, target localization, blood clearance and renal excretion—all with comparable sensitivity and accuracy.[3]

Individualized therapy planning with adjustment of injected radioactivity dose during PRRT of NETs is necessary because of high inter-patient variability in healthy organ uptake.[4] Accurate quantification of tumor uptake with Ga-68 DOTATATE PET•CT has a major impact in dosimetry for Lu-177 DOTATATE therapy. A major impact of PET/CT with Ga-68 somatostatin analogs is related to the detection of additional or unknown metastases. In comparison, SPECT- or CT-only studies often lead to just a change in management. In a study by Gabriel et al[5] involving 84 patients with suspected NET, Ga-68 DOTATOC PET/CT identified lesions that were not defined on CT in 21.4% of patients. Gabriel's study primarily relates to small bone and liver metastases. The present case also illustrates the ability of Ga-68 DOTATATE PET/CT to detect functioning metastases from NET, especially small brain metastases, which are better detected with higher matrix PET reconstruction.

Conclusion

Higher matrix reconstruction of PET data improves the target-to-background ratio of small lesions, thereby improving lesion conspicuity. Higher matrix reconstruction requires higher count statistics to decrease noise. FlowMotion technology offers acquisition of flexible ranges with variable table speeds, which enables slower acquisition with higher count statistics in regions requiring higher matrix reconstruction for increased small lesion detectability. The present case was acquired with uniform, but slower table speeds for high image quality and increased count statistics in that region in order to subsequently provide any relevant acquisition range with higher matrix reconstruction.

Examination Protocol

Scanner	Biograph mCT Flow
Injected Dose	150 MBq Ga-68 DOTATATE
Scan Delay	60 min post injection
Acquisition	Zone 1, 0.7 mm/sec
CT	Whole-body scan mode; tube voltage, 120 kV; tube current, 48 eff mAs; slice collimation, 32x1.2 mm; slice thickness, 5 mm

References:
1. **Frilling et al.** *Ann Surg.* 2010, 252: 850-856.
2. **Treglia et al.** *Endocrine.* 2012, 42: 80-87.
3. **Velikyan et al.** *J Nucl Med.* 2014, 55: 204-210.
4. **Sandstrom et al.** *J Nucl Med.* 2013, 54: 33-41.
5. **Gabriel et al.** *J Nucl Med.* 2007, 48: 508-518.

* Ga-68 DOTATATE and Lu-177 DOTATATE referenced herein are not currently recognized by the US FDA as being safe and effective, and Siemens does not make any claims regarding their use.

** Biograph mCT Flow is not commercially available in all countries. Due to regulatory reasons its future availability cannot be guaranteed. Please contact your local Siemens organization for further details.

Extension of Radiation Field Based on PET•CT in a Patient with Anal Carcinoma

By **Annika Loft, MD, PhD, and Anne Kiil Berthelsen, MD**

Data courtesy of Rigshospitalet, Copenhagen, Denmark

History

A 58-year-old male with anal squamous cell carcinoma and severe pain in the sacral region was referred for a Fludeoxyglucose F-18 (^{18}F FDG)* PET•CT study, prior to radiation therapy, for initial staging and evaluation. The study was performed on a Biograph™ mCT system 1 hour following an intravenous administration of 4 MBq/kg of body weight of ^{18}F FDG. Because of the severe pain in the sacral region, the patient was placed prone on the flat table top for the PET•CT study, which was also used for radiation therapy planning. Oral and intravenous contrast was used for the CT acquisition.

Diagnosis

^{18}F FDG PET•CT images (*Figure 1*) showed a large hypermetabolic mass that involved the full circumference of the anus and extended into the peri-anal region. The tumor extended near the sacral wall without bony invasion. As well, a small solitary hypermetabolic pre-sacral lymph node was detected above and to the left of the primary tumor.

1

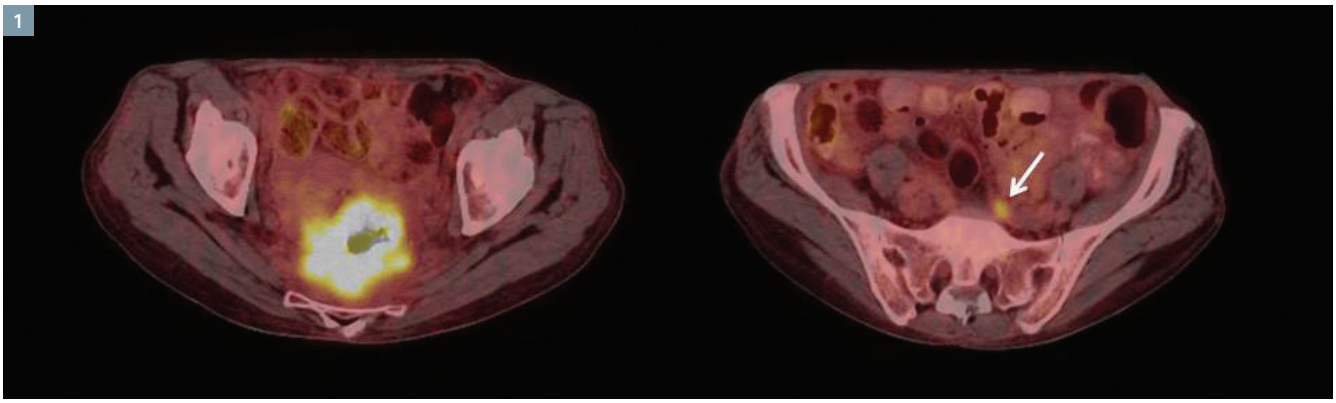

1 Transverse-fused images of the ^{18}F FDG PET•CT study show large hypermetabolic anal mass and a small solitary pre-sacral lymph node metastasis.

2

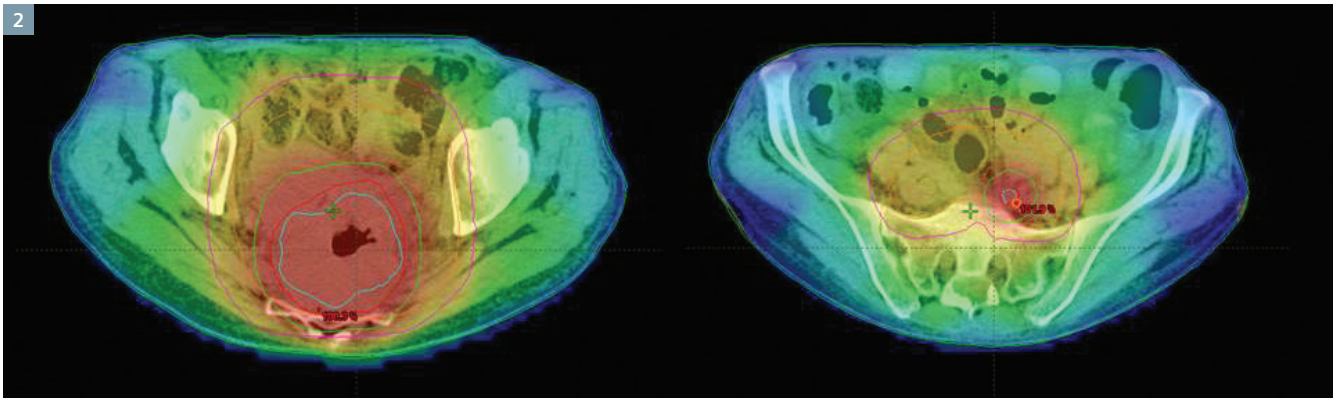

2 Radiation therapy dose color wash for different dose levels to the GTV and PTV.

With the detection of the small pelvic lymph node metastasis by PET•CT, the radiation therapy plan was altered to include the solitary pre-sacral node in the gross tumor volume (GTV).

Figure 2 shows the dose color wash from the radiation plan performed on the PET•CT-fused images with the GTV and planning target volume (PTV) defined from the PET delineated volume and extending the GTV to include the small pre-sacral lymph node metastases.

Comments

The radiation therapy field was altered in this patient based on the ^{18}F FDG PET•CT's delineation of a small pelvic metastatic node, thus leading to GTV modification. A radiation plan based purely on CT, in this case, would definitely have missed the pelvic nodal metastasis since it was normal in size on CT. A purely CT-based radiation plan in this patient would lead to low radiation to the pelvic nodal metastases, which in turn would result in a progression of the nodal metastases despite local control of the anal carcinoma.

The change in patient management, as a result of the findings, illustrates the value of ^{18}F FDG PET•CT in radiation planning for tumors in which nodal metastases and distant spread are common, as well as with local infiltration of the tumor.

Several studies have demonstrated the value of ^{18}F FDG PET/CT in radiation therapy planning for anal carcinoma. Winton et al[1] compared ^{18}F FDG PET and CT performed for initial staging and radiation planning in 61 patients with anal cancer. The staging was changed by PET in 23% of patients, with 15% being upstaged and 8% downstaged. Changes in the nodal stage were greater for tumors with a more advanced T stage. Only 14% of patients with early stage tumors had a change in the nodal stage after PET, whereas nodal stage-change was seen in 38% of patients with T3/T4 tumors after PET. PET was significantly more sensitive (89%) for nodal metastases compared to CT (62%). The incorporation of PET information into conventional imaging, including CT, changed management in 16% of cases. There was a change in treatment-intent for 3% of the patients and a change in radiation therapy fields or technique, in order to cover or exclude nodal disease, in 13% of the patients.

Mistrangelo et al[2], in a similar study, showed almost 50% higher sensitivity for detecting perirectal and pelvic nodal metastases with PET/CT when compared to staging with CT. PET/CT upstaged 37.5% of patients and downstaged 25% of patients. Radiation fields were changed in 12.6% of patients based on PET/CT findings.

As adopted in this clinical study, contrast-enhanced CT is often combined with PET in order to better delineate tumors and blood vessels. Contrast-enhanced CT with PET has shown to be advantageous in staging anal carcinoma when compared to PET or CT only.[3] In this study, contrast-enhanced PET/CT was instrumental in the changing of radiotherapy fields for 23% of the patients, when compared to CT or PET results alone. PET identified lesions not seen on CT in 14% of the patients. While in 8% of the patients, only contrast CT was able to detect metastatic lesions.

These studies highlight the role of ^{18}F FDG PET•CT in accurate staging of anal cancer as well as its impact on radiation therapy for a substantial percentage of patients.

Conclusion

PET•CT provides comprehensive information about the tumor's extent and margins, infiltration into surrounding tissues, as well as nodal and distant metastases—all of which help guide therapy decisions and radiation plans. Although the ^{18}F FDG uptake in the involved iliac lymph node is low, the high lesion-contrast, provided by time-of-flight PET acquisition, clearly delineates the involved node.

Examination Protocol

Scanner	Biograph mCT 64
Injected Dose	370 MBq of ^{18}F FDG
Scan Delay	60 min post injection
Acquisition	3 min/bed
CT	Whole-body scan mode; tube voltage, 120 kV; tube current, 225 eff mAs; slice collimation, 32x1.2 mm; slice thickness, 3 mm

References:
1. **Winton et al.** *British Journal of Cancer.* 2009. 100: 693-700.
2. **Mistrangelo et al.** *Int J Radiat Oncol Biol Phys.* 2012, Sep 1. 84(1): 66-72.
3. **Bannas et al.** *Int J Radiat Oncol Biol Phys.* 2011, Oct 1. 81(2): 445-451.

* Indications and important safety information on Fludeoxyglucose F 18 injection can be found on page 05. The full prescribing information can be found on pages 38-40.

Choline PET•CT Detection of Metastases in a Patient with Primary Prostate Carcinoma

By **Olivier Rager, MD**

Data courtesy of Hospital University of Geneva, Geneva, Switzerland

History

A 75-year-old man presented with intermittent urinary obstruction and a clinical and rectal ultrasound-guided, biopsy-based diagnosis of adenocarcinoma of the prostate. A Gleason score of 9 (4 + 5) suggested aggressive, poorly differentiated prostate cancer. The serum PSA was very high (16 ng/ml). Due to the high PSA and histopathological grading for aggressive prostate cancer, the patient underwent a Choline PET•CT. Within 5 minutes following an IV injection of 550 MBq of Choline, the PET•CT study began. The study was performed on a Biograph mCT Flow™** system with continuous-bed-motion acquisition at a uniform speed of 0.7 mm/sec. The acquisition was in the caudocranial direction.

Diagnosis

As shown in *Figure 1-3*, Choline PET•CT demonstrated high tracer accumulation in the primary prostate tumor. This involved both lobes and multiple pelvic lymph node metastases that involve the bilateral internal iliac group and para-rectal nodes. Also, metastatic lymph nodes were visible in the left para-aortic nodal group at the level of the left kidney. Two small focal skeletal metastases showing prominent uptake of Choline were visible in the left pubic bone and right ileum.

1 Whole-body MIP image of Choline PET•CT shows high physiological uptake in the liver, pancreas, salivary glands, kidneys and marrow. Focal uptake in the prostate bed and pelvis suggested a primary prostate tumor with pelvic metastases.

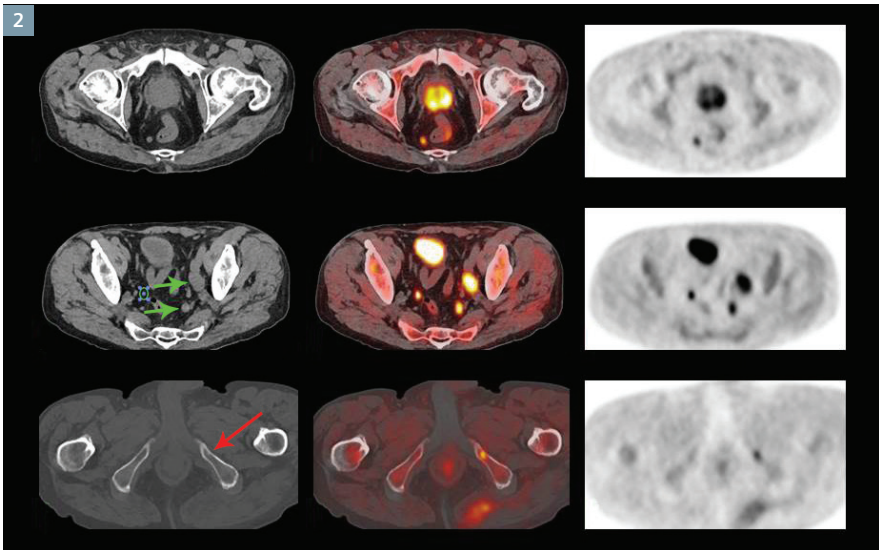

2 CT and fused PET•CT images show increased uptake in the primary prostate tumor along with multiple small pelvic nodal metastases—right pararectal, left internal iliac (*green arrows*) and right internal iliac (*circle near green arrows*)—as well as a small focal area of uptake in the left pubic bone, which suggested of skeletal metastases.

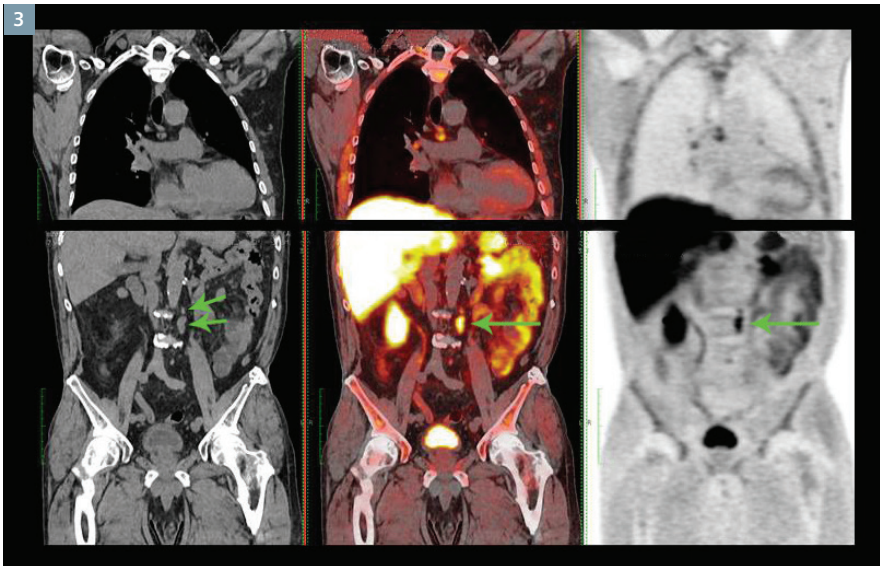

3 Coronal CT and fused PET•CT images show hypermetabolic left para-aortic lymph node metastases (*green arrows*) along with high physiological uptake in the liver, kidneys and bowel loops. Small focal nodal uptake in the mediastinum and left axilla were probably related to reactive hyperplasia, which occasionally shows Choline accumulation. Small focal bony metastases were delineated in the right ileum just above the acetabulum.

Comments

Choline PET•CT demonstrated, in this patient, pelvic and para-aortic lymph nodal metastases and several bone metastases, with a poorly differentiated primary prostate cancer that had a high Gleason score and increased serum PSA. Choline demonstrated a high metastatic lesion burden, suggesting an adverse prognosis, which is instrumental in anti-androgen therapy decisions. Choline PET•CT shows a high sensitivity in the presence of high-serum PSA and fast PSA kinetics. In this patient with aggressive primary tumor histopathology and high-serum PSA, Choline PET•CT demonstrated 6 lymph node metastases and 2 bone metastases. This correlates with the disease burden expected from the high-serum PSA. One of the lymph node metastases (right internal iliac nodal group) shows sub-centimeter size on CT, but showed high Choline uptake on PET, thereby highlighting the value of Choline PET in detecting early pelvic nodal metastases. In the primary prostate carcinoma, Choline PET•CT showed a low sensitivity of around 60% for the pelvic lymph node metastases detection, but with high specificity.[1] The detection rate has been closely correlated with serum PSA. In a study comparing Choline PET/CT detection rate for recurrent prostate cancer with serum PSA, the detection rate was 43% for PSA of 1-2 ng/ml while it was 73% for PSA >3 ng/ml.[2]

Apart from the Gleason score and serum PSA, the number of metastases in a patient with primary or recurrent prostate cancer has major prognostic implication. Singh et al[3] reported that patients with up to 5 metastases had a 5-year overall survival of 73%, which is significantly better than patients with more than 5 metastases (45%). Oligometastatic patients may harbor tumors that are biologically less aggressive with limited metastatic potential and a slow growth rate. These patients may be suitable for more aggressive treatment approaches.

Conclusion

Detection of small lymph nodal metastases with Choline PET•CT with continuous bed motion can help define the overall disease burden and determine the oligometastatic status of a patient in order to determine candidates for more aggressive therapy.

Examination Protocol

Scanner	Biograph mCT Flow Edge 128
Injected Dose	550 MBq of radiolabelled Choline
Scan Delay	5 min post injection
Acquisition	0.7 mm/sec
Injected Dose	Whole-body scan mode; tube voltage, 120 kV; tube current, 55 eff mAs; slice collimation, 32x1.2 mm; slice thickness, 2 mm

References:
1. **Schiavina et al.** *Eur Urol.* 2008. 54(2): 392-401.
2. **Krause et al.** *Eur J Nucl Med Mol Imaging.* 2008. 35: 18-23.
3. **Signh et al.** *Int J Radiat Oncol, Biol, Phys.* 2004. 58: 3-10.

* Biograph mCT Flow is not commercially available in all countries. Due to regulatory reasons its future availability cannot be guaranteed. Please contact your local Siemens organization for further details.

Evaluation of Response to Radiation Therapy (IMRT) using Choline PET•CT in a Patient with Metastatic Prostate Carcinoma

By **Richard Baum, MD, PhD**

Data courtesy of Bad Berka Zentralklinic, Bad Berka, Germany

History

A 75-year-old man, with a history of adenocarcinoma of prostate that was treated with prostatectomy two years prior, presented with gradual and progressive increases in serum PSA. The patient was referred for Choline PET•CT, because metastases were a possibility.

Choline PET•CT was performed on a Biograph™ mCT system 60 minutes following an intravenous administration of the tracer. An initial contrast-enhanced CT was performed, followed by a whole-body PET acquisition at 3 minutes per bed position.

Diagnosis

Choline PET•CT demonstrated (*Figure 1*) two distinct, metabolically active, slightly enlarged para-aortic lymph node metastases at the level of the lower pole of the kidneys. The prostatic bed, periprostatic zones, pelvis and region of the aortic bifurcation did not show any abnormal uptake. Physiological uptake in the liver, kidneys, pancreas, salivary glands and bone marrow were normal.

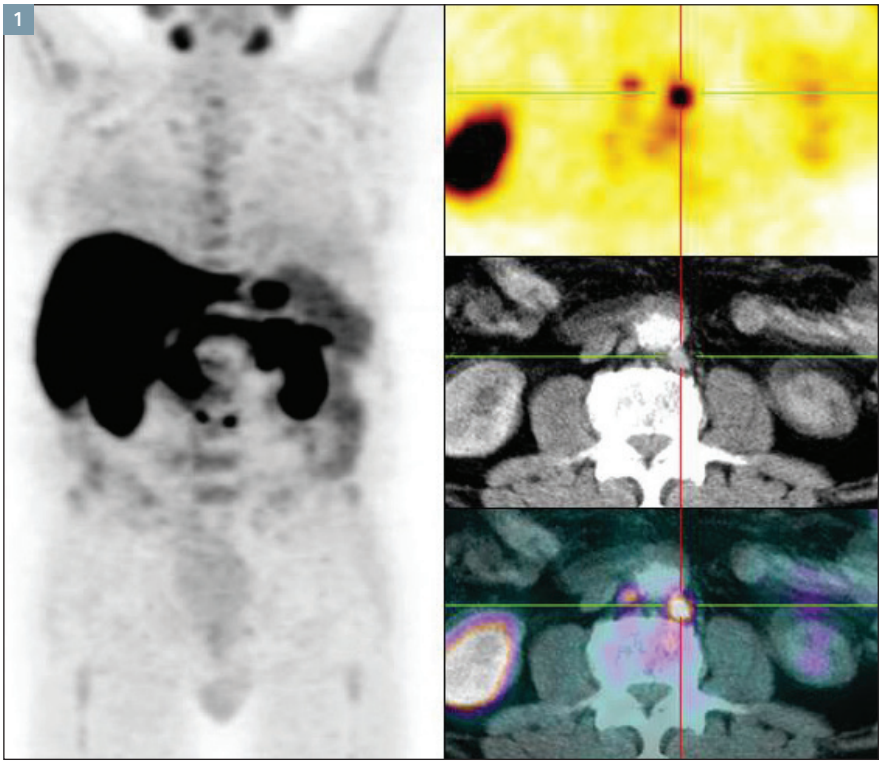

1 Choline PET•CT shows focal increase in uptake in two para-aortic nodal metastases at the level of the lower pole of the kidneys. No abnormality was detected in the prostatic bed, periprostatic zone or the rest of the pelvis.

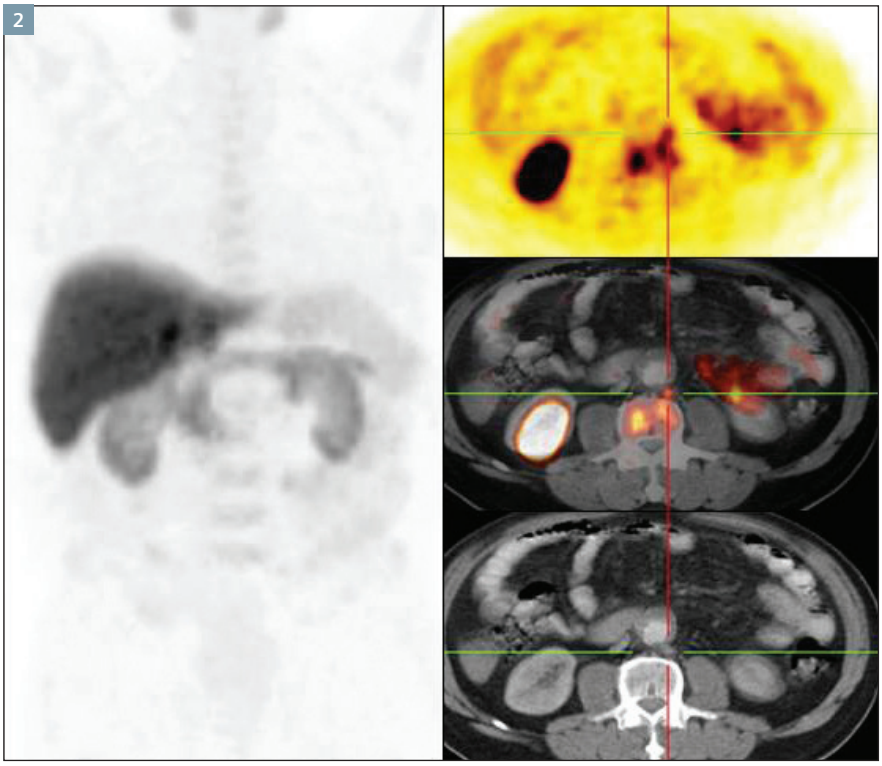

2 Follow-up Choline PET•CT performed three months post-IMRT shows significant decrease in size and intensity of tracer uptake in the para-aortic lymph node, suggesting a positive response to therapy.

Due to the metastatic nodes defined by Choline PET•CT, the patient underwent radiation therapy using intensity modulated radiation therapy (IMRT) for the abdominal lymph node metastases. Following IMRT, there was a quick decrease in serum PSA. 3 months after the completion of IMRT, the patient underwent a follow-up Choline PET•CT. Serum PSA was normal at the time of the follow-up study.

Follow-up Choline PET•CT showed a significant decrease in size and intensity of tracer uptake in both metastatic para-aortic lymph nodes (*Figure 2*). The node on the right side of the aorta had almost disappeared, while the left-sided metastatic node had decreased considerably in size and showed much lower intensity of uptake. No other new PET-positive lesions were visible.

Comparison images at the same slice levels of the pre- and post-therapy Choline PET•CT studies (*Figure 3*) showed the decreasing degree in size and intensity of tracer uptake in the metastatic nodes post-IMRT, thereby confirming a positive therapy response which was also reflected by the normalization of serum PSA.

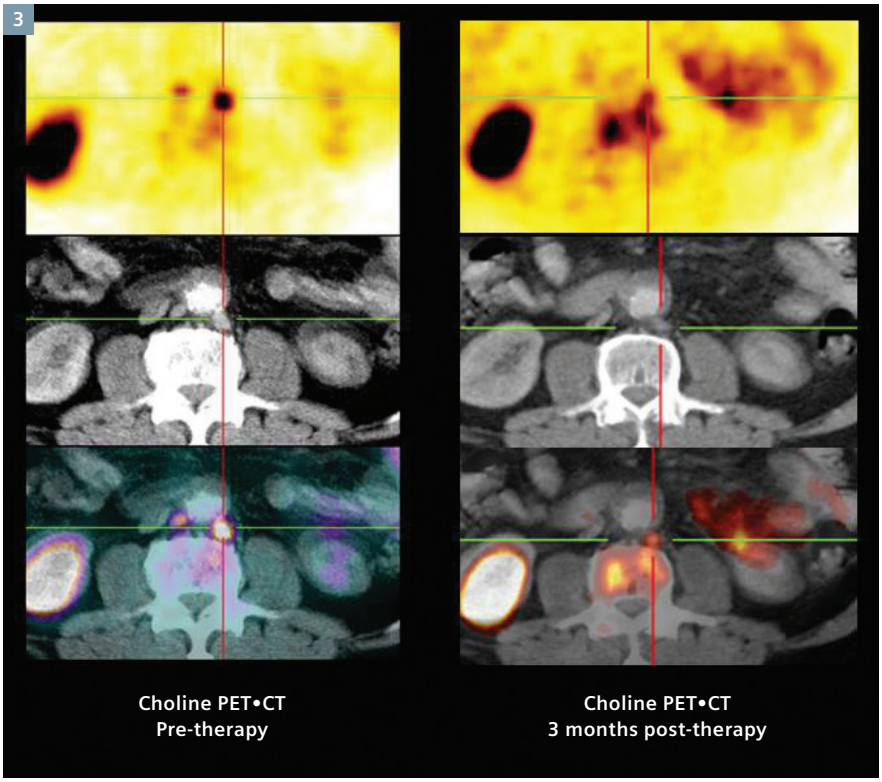

3 A side-by-side comparison of pre-therapy and three months post-therapy Choline PET•CT images shows significant decrease in size and uptake intensity of metastatic lymph nodes.

Comments

This clinical example demonstrates the use of Choline PET•CT in the detection of recurrent prostate carcinoma and for monitoring therapy. Choline is incorporated into malignant cells by conversion into phosphorylcholine, which is then trapped inside the cell. This is followed by a synthesis of phosphatidylcholine, which constitutes a main component of cell membranes. Increased Choline uptake in prostate cancer cells reflects increased cell proliferation in tumors and by up-regulation of Choline kinase in cancer cells. Thus, the uptake of radiolabelled Choline in malignant tumors represents the rate of tumor cell proliferation.

Biochemical recurrence reflected by a rise in PSA occurs in 20-40% of patients within 10 years of definitive radical prostatectomy or radiation therapy, usually preceding a clinically detectable disease. After radical prostatectomy, PSA should fall to undetectable values within 3 to 4 weeks, while the PSA level decreases more slowly after radiation therapy. A shorter PSA doubling time (<10 months) after radical prostatectomy or radiation therapy is a strong indicator for recurrence.[1] Choline PET has been shown to be useful for detecting recurrence in patients with PSA relapse. Rinnab et al[2] evaluated the detection of biochemical recurrence of prostate cancer after radical prostatectomy with C-11 Choline PET/CT in 41 patients, and reported a sensitivity of 89% for patients with a PSA <2.5 ng/ml. Sensitivity was 75% for patients with PSA 1.5-2.5 ng/ml, while it was 100% for patients with PSA >5 ng/ml.

Most studies evaluating Choline PET in the biochemical relapse of prostate cancer have demonstrated high sensitivity in patients with higher PSA levels and PSA doubling time. In a large prospective study, Cimitan et al[3] detected prostate cancer recurrence with ^{18}F-FCH PET/CT in 53 of 100 patients with PSA relapse. Of the patients with false negative studies, 89% had a serum PSA level <4 ng/ml. The authors concluded that ^{18}F-FCH PET/CT is not likely to have a significant impact on the care of prostate cancer patients with biochemical recurrence until PSA increases to above 4 ng/ml. The correlation between the detection rate of C-11 Choline PET/CT and the serum PSA level is drawn to attention by this study.

Krause et al[4], in a study involving 63 prostate cancer patients with biochemical relapse, demonstrated a significant correlation between C-11 Choline PET/CT detection rate and PSA serum levels. The detection rate was 36% for a PSA value <1 ng/ml, but 73% for a PSA value greater than or equal to 3 ng/ml. The overall detection rate for PET was 59%.

Castellucci et al[5] evaluated the correlation of total PSA, PSA velocity and PSA doubling time on C-11 Choline PET/CT detection rate in 190 patients that were treated with radical prostatectomy if there was evidence of biochemical failure. The C-11 Choline PET/CT detection rate was 67% in patients with PSA >5 ng/ml, while it was only 19% in the group with PSA <1 ng/ml. Similarly, the detection rate was 70% in the group with PSA velocity >5 ng/ml/yr and 60% with PSA doubling time of <2 months, while the detection rates were low with PSA velocity of 1 ng/ml/yr and PSA doubling time >6 months. In a different study, Castellucci et al[6] evaluated the correlation of PSA kinetics and recurrence detection rate with C-11 Choline PET/CT in a patient population with biochemical relapse and low PSA levels. Detection rates were higher in patients with fast PSA kinetics (PSA doubling time of 4.34 months) compared to patients with slow PSA doubling time of 13.3 months, even when total PSA was <1.5 ng/ml. This study suggests that Choline PET/CT could be an effective tool for recurrence detection even in patients with low-serum PSA if the PSA kinetics are fast, which may help improve patient selection of Choline PET/CT.

Apart from recurrence detection in patients with biochemical failure following definitive therapy in prostate cancer, Choline PET/CT has been used for evaluation of therapy response in primary as well as recurrent tumor. Challapalli et al[7] evaluated sequential Choline PET/CT in primary prostate cancer undergoing radical prostate radiotherapy with concurrent androgen deprivation and found a significant correlation between changes in SUV_{max} and serum PSA. However, there was a larger average reduction of serum PSA (94%) following therapy compared to that in tumor SUV_{max} (58%).

Conclusion

Choline PET•CT in this patient was instrumental in detecting para-aortic nodal metastases. The high-serum PSA of 5.7 ng/ml puts the patient in a group in which Choline PET/CT has shown high sensitivity. Due to the high sensitivity of Choline PET/CT in patients with biochemical recurrence with this level of PSA, the delineation of para-aortic metastases without evidence of prostatic bed recurrence or other pelvic nodal metastases gives confidence to the oligometastatic status of this patient and justifies external beam radiation therapy to the involved nodes. Choline PET•CT also shows efficacy in accurate evaluation of response to radiation therapy as demonstrated by the decrease in size and uptake intensity of the involved nodes 3 months post-IMRT. This correlates with the normalization of serum PSA. However, there is slight tracer uptake in one of the nodes in the post-therapy PET•CT that may reflect post-radiation reactive changes due to the biochemical evidence that demonstrates an absence of residual tumor since serum PSA is normalized post-therapy.

Examination Protocol

Scanner	Biograph mCT 64
Injected Dose	550 MBq radiolabelled Choline
Scan Delay	60 min post injection
Acquisition	3 min/bed
CT	Whole-body scan mode; tube voltage, 120 kV; tube current, 55 eff mAs; slice collimation, 32x1.2 mm; slice thickness, 2 mm

References:
1. **Bouchelouche.** *Semin Nucl Med.* 2011. 41(1): 29-44.
2. **Rinnab et al.** *World J Urol.* 2009. 27: 619.
3. **Cimitan et al.** *Eur J Nucl Med Mol Imaging.* 2006. 33(12): 1387-1398.
4. **Krause et al.** *Eur J Nucl Med Mol Imaging.* 2008. 35: 18-23.
5. **Castellucci et al.** *J Nucl Med.* 2009. 50: 1394-1400.
6. **Castellucci et al.** *Eur J Nucl Med Mol Imaging.* 2011. 38(1): 55-63.
7. **Challapalli et al.** *Nucl Med Commun.* 2014. 35(1): 20-29.

Improved Characterization of Ischial Tendinitis using xSPECT Bone

By **Harun Ilhan, MD**

Data courtesy of Ludwig-Maximilians University, Munich, Germany

History

A 62-year-old female with a history of breast carcinoma who was treated with mastectomy and local radiation therapy had subsequently developed lung metastases, resulting in partial resection of the affected lung tissue. Recently, the patient presented with pain in the pelvis. A CT scan performed at a private clinic was reported as suspicious for metastases in the right ischium and sacro-iliac joint. The patient underwent ^{99m}Tc MDP bone scintigraphy with xSPECT* for further diagnostic workup.

Following a 650 MBq IV injection of ^{99m}Tc MDP, the patient underwent an initial whole-body planar bone scan, followed by an xSPECT study of the pelvis. A low-dose CT was used as an integrated procedure with the SPECT study. A comparison of standard 3D OSEM iterative reconstruction and xSPECT images was performed, along with the review of CT and fused images for interpretation.

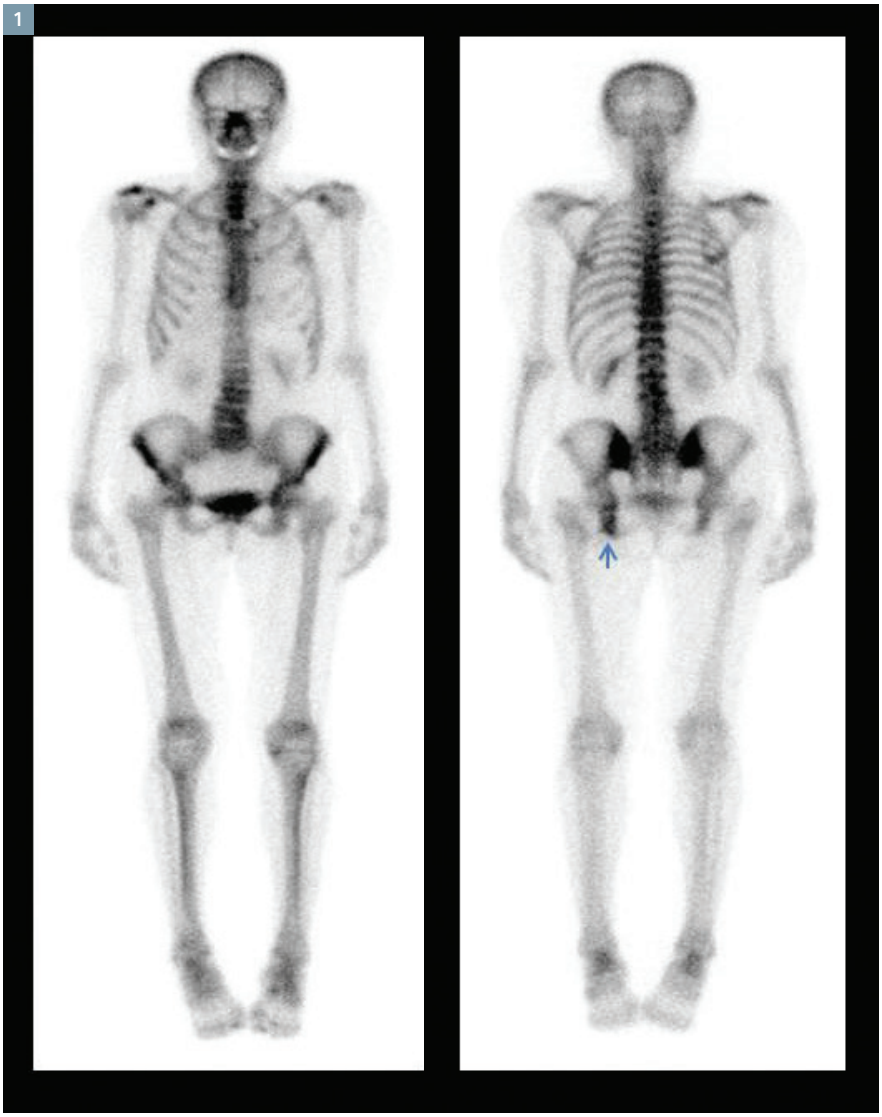

1 A planar whole-body bone scan shows increased uptake in the left ischium.

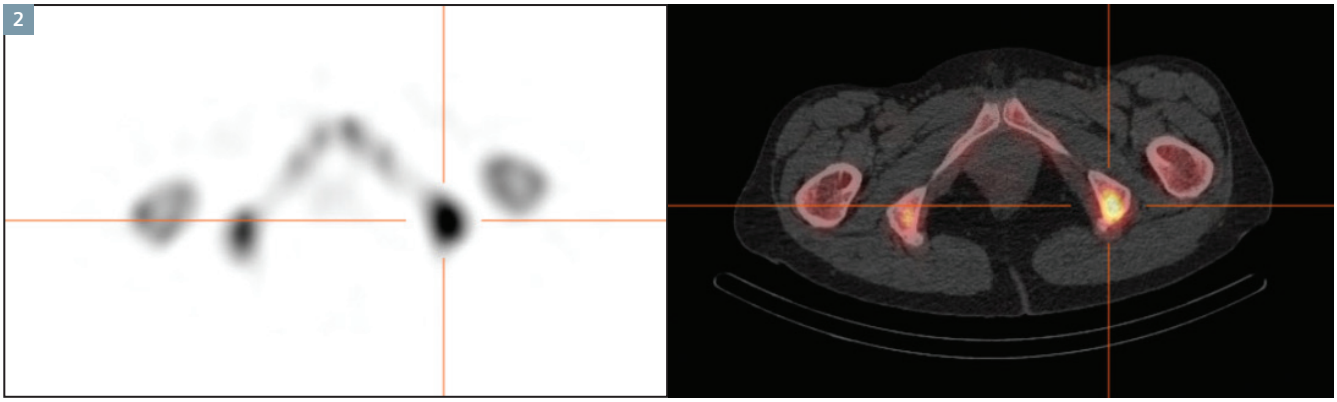

2 CT and 3D OSEM reconstruction of ^{99m}Tc MDP bone SPECT (*right*) of the pelvis shows focal hypermetabolism of tracer in the left ischial tuberosity without any significant CT changes.

Diagnosis

The whole-body planar bone scan (*Figure 1*) showed increased uptake in the left ischial tuberosity (*arrow*). As well, slightly increased uptake in the left acetabulum was apparent. Both sacro-iliac joints showed normal uptake. Tracer uptake in the acromio-clavicular and sternoclavicular joints demonstrated degenerative changes. The rest of the skeletal system showed a normal tracer distribution.

3D OSEM reconstructions of the pelvis (*Figure 2*) showed increased tracer uptake in the whole of the left ischial tuberosity, without any significant sclerosis or lytic region on CT. No soft tissue changes were visible on the low-dose CT. The pattern of ischial hypermetabolism seen on 3D iterative-reconstructed images was equivocal since it involved the whole of the ischial tuberoisty, including the cortical and the spongy bone.

Although there were no significant CT changes, the pattern of uptake involving the entire cross section of the ischium reflected the possibility of early metastases.

xSPECT Bone* images of the pelvis (*Figure 3*) showed sharp delineation in the area of focal hypermetabolism, in the left ischial tuberosity, which localized exactly to the outer and medial cortex with relatively lower uptake in the spongy bone. This pattern of uptake suggested a benign pathology, possibly a periosteal reaction following tendon injury, tendon inflammation or cortical shear stress due to trauma. Such predominant cortical uptake as seen in xSPECT Bone is uncommon with bone metastases that usually begin in the marrow and cause a blastic or lytic response associated with hypermetabolism, which usually involves both spongy and cortical bone. As shown in *Figure 4*, standard 3D iterative reconstruction was not able to differentiate cortical from spongy bone uptake like xSPECT Bone was able to within the lesion in the ischial tuberosity.

The patient subsequently underwent contrast MRI and demonstrated contrast enhancement within the tendinous insertion of the lateral pelvic wall muscles into the ischial tuberosity (*Figure 5*). The cortex and spongy bone within the ischial tuberosity did not show hyper-intensity on T1 or contrast enhancement, suggesting an absence of major bony or marrow pathology. Due to the contrast enhancement in the tendon insertion to the ischial tuberosity, the lesion appeared to be related to a tendinitis with reactive cortical changes in the ischial tuberosity.

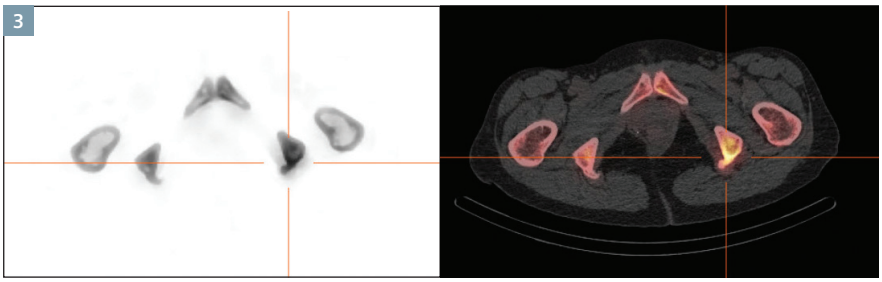

3 CT and xSPECT Bone images (*right*) of the pelvis show the area of increased uptake predominantly localized to the outer edge of the medial cortex of the ischial tuberosity with less involvement of the spongy bone.

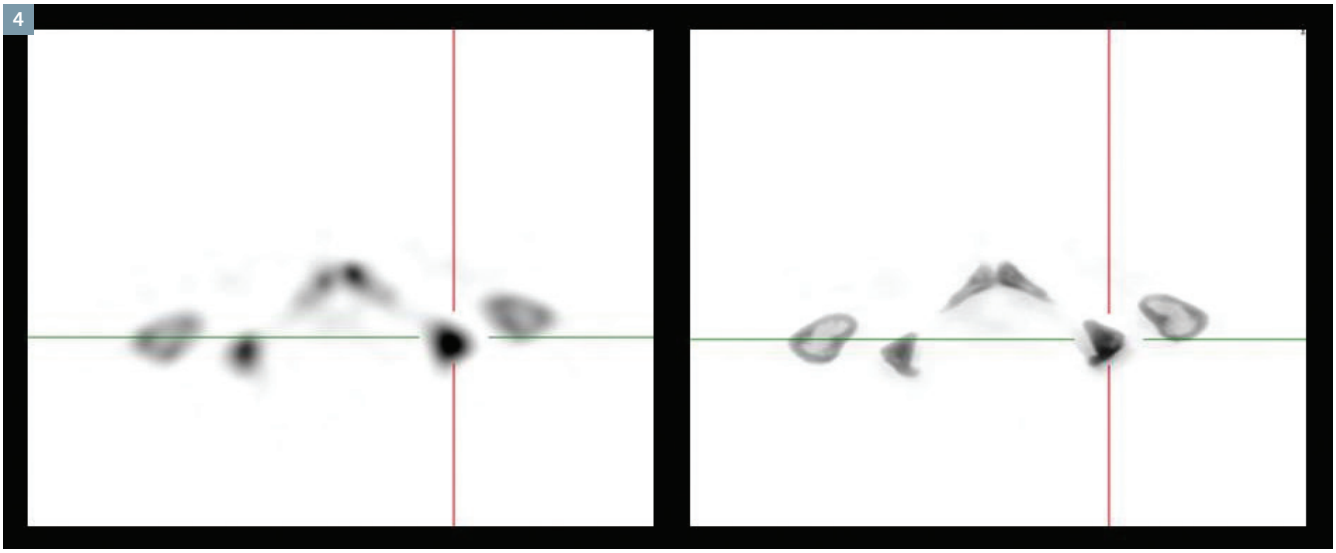

4 3D iterative-reconstructed (*left*) and xSPECT Bone (*right*) images shown at the same slice level demonstrate xSPECT Bone's sharp localization in the area of increased tracer uptake, as seen in the medial part of the cortex of left ischial tuberosity with relatively lower uptake within the spongy bone. This suggested a predominantly linear cortical pathology. In comparison, the 3D iterative-reconstructed image shows uniform increased uptake involving the whole of ischial tuberosity without any differentiation of uptake between the cortex and medulla.

Comments

3D iterative reconstruction of bone SPECT in this case defined a hypermetabolic lesion involving the entire cortical and spongy bone components of the ischial tuberosity. Even in the absence of any significant findings in the low-dose CT, which would suggest osteoblastic or osteolytic activity, this pattern of uptake suggested metastases in a patient with known history of breast carcinoma with lung metastases. However, xSPECT Bone images showed sharply defined uptake in the cortical bone, and localized the increased uptake to the medial and outer cortex. This suggested a benign pathology and pointed to some periosteal inflammation, which is commonly caused by inflammation or trauma in the tendon insertion to the bone or to cortical shear stress that may be related to trauma. The MRI showed contrast enhancement in the tendon insertion, with an absence of pathology within the bone of the ischial tuberosity, which confirmed the suspicion of tendinopathy, secondary to tendon inflammation at the level of its insertion to the bone. xSPECT Bone facilitated the interpretation of the bony uptake due to the differentiation between uptake in the cortical and spongy bones.

5

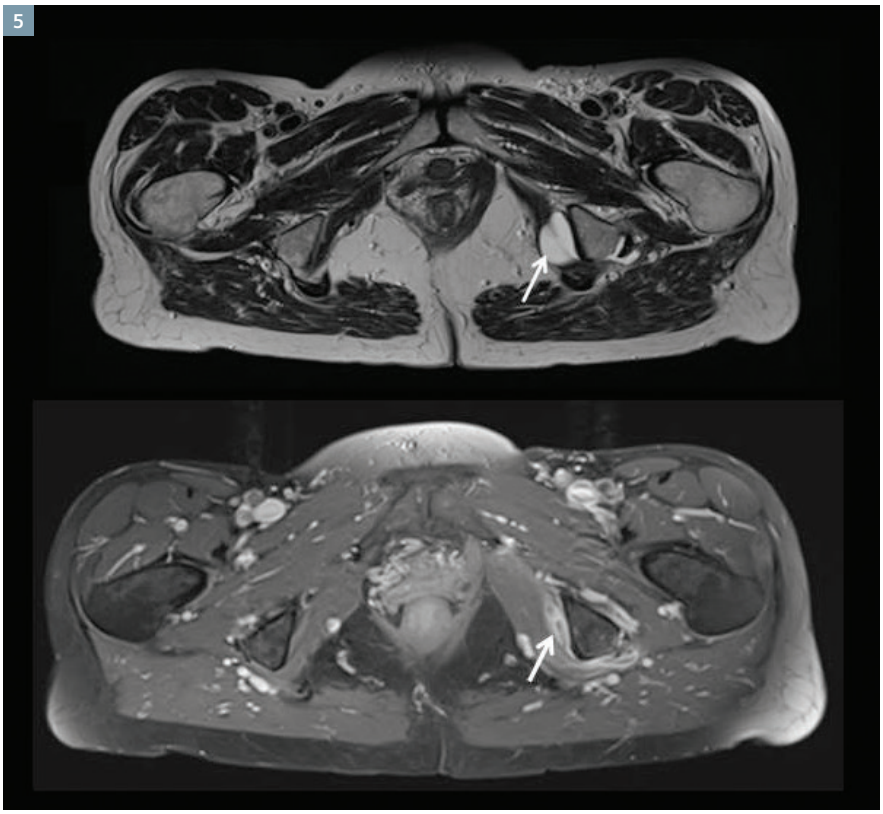

5 T1 (*top row*) and post-Gadolinium fat suppressed (*bottom row*) transverse MRI images through the left ischial tuberosity show hyperintensity and contrast enhancement around the insertion of the tendons of the internal obturator and other muscles of the lateral pelvic wall. *Data courtesy of the Institute of Clinical Radiology, University of Munich, Munich, Germany; Clinical director: Prof. Dr. med. Dr. h.c. Maximilian Reiser, FACR, FRCR.*

Conclusion

xSPECT Bone reconstruction sharply defined uptake in the cortical bone, which suggested a benign pathology. Sharp definition improves diagnostic confidence in excluding more serious conditions.

Examination Protocol

Scanner	Symbia Hybrid System
Injected Dose	650 MBq of ^{99m}Tc DPD
Scan Delay	3 hours post injection
Parameters	SPECT: 32 stops, 20 sec/stop
CT	130 kV, 50 eff mAs, 3 mm slice thickness

* xSPECT and xSPECT Bone are not commercially available in all countries. Due to regulatory reasons their future availability cannot be guaranteed. Please contact your local Siemens organization for further details.

The statements by Siemens customers described herein are based on results that were achieved in the customer's unique setting. Since there is no "typical" hospital and many variables exists (e.g., hospital size, case mix, level of IT adoption) there can be no guarantee that other customers will achieve the same results.

Delineation of Severe Osteochondrosis with xSPECT Bone

By **Torsten Kuwert, MD, Director of Nuclear Medicine**

Data courtesy of the Department of Nuclear Medicine, University of Erlangen, Erlangen, Germany

History

A 62-year-old female patient presented with severe back pain. The patient was referred for a ^{99m}Tc DPD bone scan to evaluate for spinal pathology. A 3-phase bone scan was performed. Delayed images were 3 hours after administration of 375 MBq (10 mCi) of ^{99m}Tc DPD. Conventional 3D iterative and xSPECT Bone* images were reconstructed and compared, along with fusion of CT and SPECT.

Diagnosis

First and second phases of the 3-phase bone scan were unremarkable. Delayed SPECT showed increased uptake of the tracer in the L3-L4 lumbar vertebral end plates and intervertebral disc. xSPECT Bone showed sharp delineation of the individual vertebrae with clear definition of the focal area of increased uptake within the L3-L4 intervertebral joint, and adjacent vertebral end plates on the left side and, to a lower extent, in the L4-L5 on the right side. xSPECT* clearly defined the location of the uptake and delineated the sharp vertebral end plate margins, thereby demonstrating a narrowing of the L3-L4 intervertebral disc space. Other lumbar vertebrae showed normal shape and normal intervertebral disc spaces without abnormal focal uptake.

Low-dose CT showed narrowing of L3-L4 intervertebral disc space with severe erosion of the adjacent vertebral end plates, along with mild sclerosis. xSPECT and CT-fused data showed increased uptake limited to the zone of sclerosis, adjacent to the vertebral end plate erosion. The other intervertebral disc spaces appeared normal without abnormally increased uptake or end plate changes on the CT. Minor degenerative changes were visible in the lateral aspect of L4-L5 vertebral end plates.

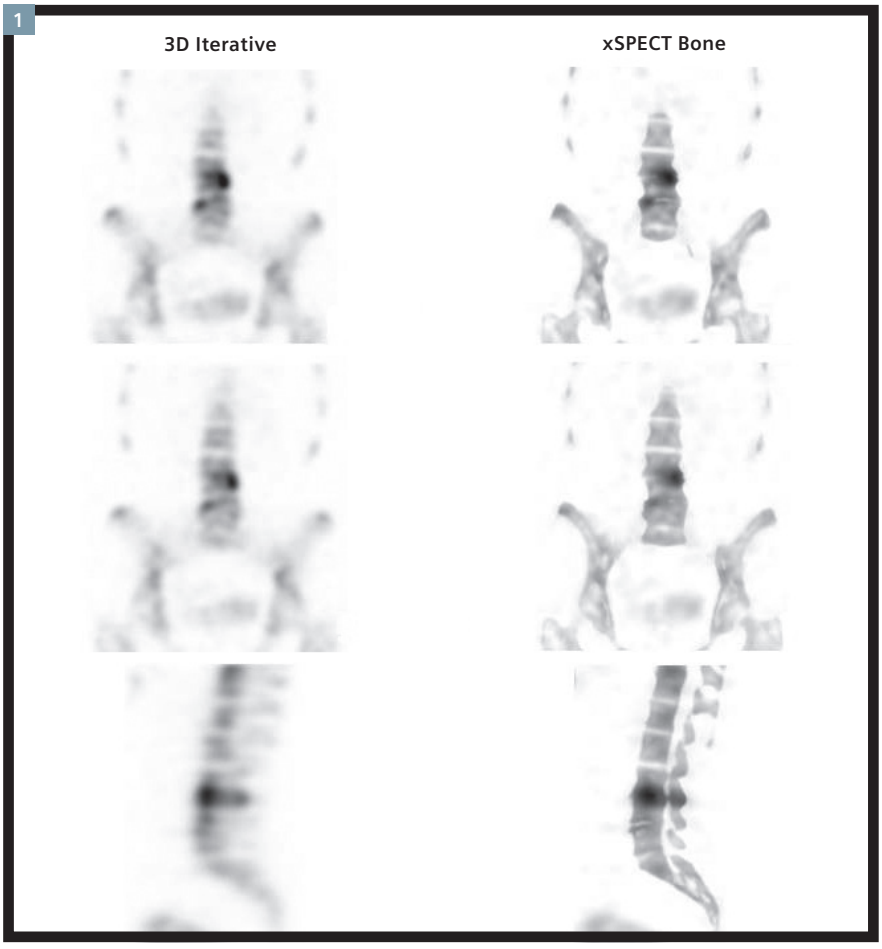

1 Comparison of 3D iterative, CT-attenuation-corrected, SPECT reconstruction and xSPECT Bone reconstruction shows increased uptake within the L3-L4 intervertebral joint and eroded adjacent vertebral end plates.

Comments

The clinical presentation of the patient, along with the standard 3D iterative SPECT findings of narrowing disc space, end plate erosion and severely increased bone metabolism in the adjacent vertebral end plates without major involvement of other intervertebral disc spaces, suggested severe disc space degeneration or osteochondrosis. The intensity of end plate tracer uptake was clearly higher than the degree of sclerosis, which supported the diagnosis of active osteochondrosis.

Conclusion

Compared to standard attenuation-corrected SPECT reconstruction, xSPECT Bone images clearly delineated in the intervertebral disc spaces and uptake patterns, and helped interpret the degree and extent of intervertebral disc degeneration and the correlation of uptake intensity to the degree of erosion and sclerosis. This level of delineation with xSPECT Bone helped define the severity of osteochondrosis.

2

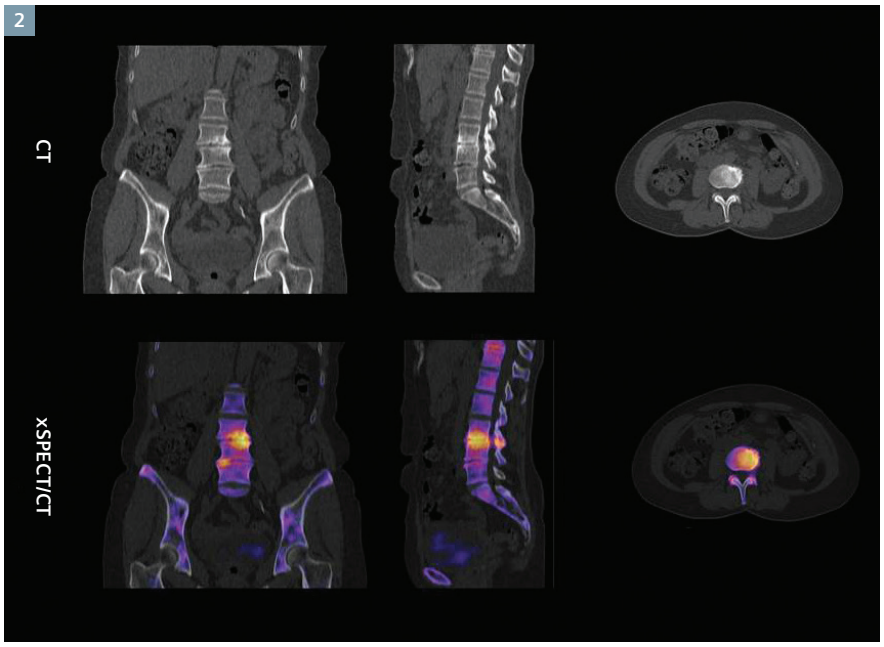

2 xSPECT/CT examination reveals an active osteochondrosis in L3-L4 as well as an arthrosis of the facet joints on both sides. Additionally, the beginning of an osteochondrosis in L4-L5 is visible.

Examination Protocol

Scanner	Symbia™ with xSPECT Bone
Injected Dose	375 MBq (10 mCi) of ^{99m}Tc DPD
Scan Delay	3 hours post injection
Parameters	60 frames, 15 sec/frame
CT	130 kV, 30 ref mAS, 5 mm slice thickness

* xSPECT and xSPECT Bone are not commercially available in all countries. Due to regulatory reasons their future availability cannot be guaranteed. Please contact your local Siemens organization for further details.

The statements by Siemens customers described herein are based on results that were achieved in the customer's unique setting. Since there is no "typical" hospital and many variables exists (e.g., hospital size, case mix, level of IT adoption) there can be no guarantee that other customers will achieve the same results.

Femoral Osteoid Osteoma Delineated by ^{99m}Tc MDP xSPECT Bone

By **Antonio Garcia, MD, Department of Nuclear Medicine**

Data courtesy of Manila Doctors Hospital, Manila, Philippines

History

A 27-year-old female presented with gradually progressive hip pain. The pain was nocturnal, often severe and appeared to radiate down to the lower extremities. An MRI of the lumbar spine showed mild L4-L5 disc bulge, but the pain did not improve with rest and traction. The patient underwent a ^{99m}Tc MDP bone scan to evaluate skeletal pathology. An xSPECT Bone* study was performed on a Symbia Intevo™* 16 scanner following a 20 mCi injection of ^{99m}Tc MDP. A multi-bed SPECT study was performed for the thoracic and lumbar spine and pelvis. The study was reconstructed using 3D iterative reconstruction and xSPECT Bone.

Diagnosis

xSPECT Bone showed a focal area of increased uptake in the upper femoral shaft, involving the anterior and lateral part of the cortex and adjacent marrow (*Figure 1* and *2*). There was also a mild and diffuse increased uptake in both the cortex and marrow above the focal hot area, extending up to the level of the lesser trochanter. The rest of the femoral shaft and the head and neck of the femur showed normal uptake.

CT and fusion of xSPECT Bone and CT (*Figure 3-5*) showed diffuse variegated sclerosis in the upper femoral shaft involving the marrow and extending up to the level of lesser trochanter, along with cortical thickening and mild erosion and irregularity of the anterior and lateral cortex. The focus with the maximum intensity of skeletal hypermetabolism in the upper part of femoral shaft co-registered

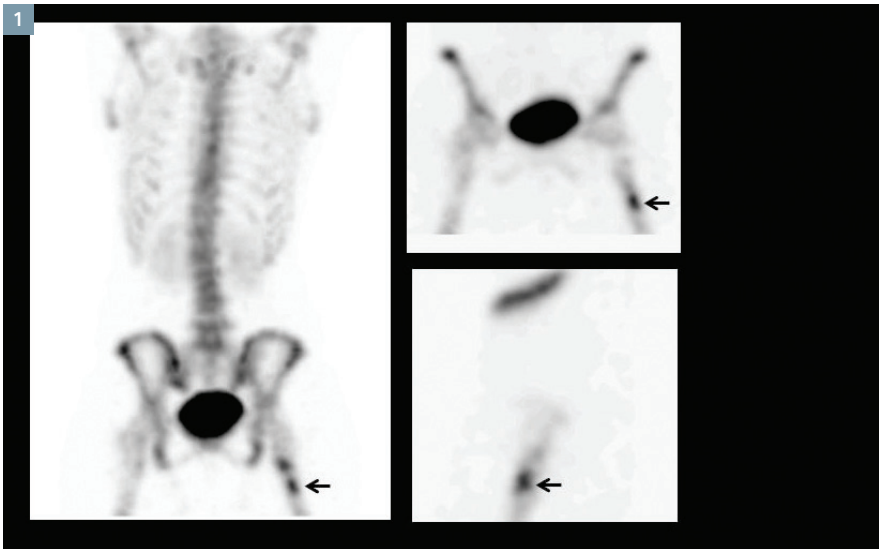

1 SPECT MIP and MPR images using 3D iterative reconstruction show a focal hot area in the upper part of the shaft in the left femur (*arrows*). Cornal and sagittal MPR images show the focal uptake involving both the anterolateral cortex and the marrow.

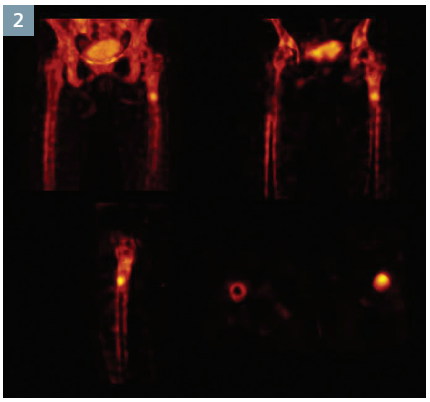

2 xSPECT Bone images show sharp delineation of focal increase of uptake of ^{99m}Tc MDP in the upper part of the left femoral shaft, involving the anterior and lateral part of the cortex and the marrow. Note the sharply delineated cortical margins in the femoral shaft with xSPECT Bone.

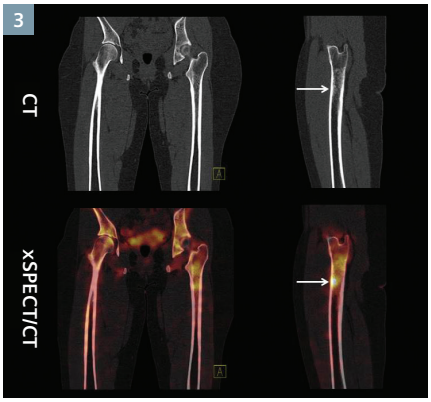

3 CT shows mild diffuse variegated sclerosis within the marrow, with minor thickening of the cortex, especially at the level of the focal area of high ^{99m}Tc MDP uptake (*arrow*). Fusion of CT and xSPECT Bone shows a focal hot area in ithe anterior and lateral aspect of the femoral shaft, adjacent to the cortex with mild uptake that corresponds to the mild sclerosis above the hot region and up to the level of the lesser trochanter.

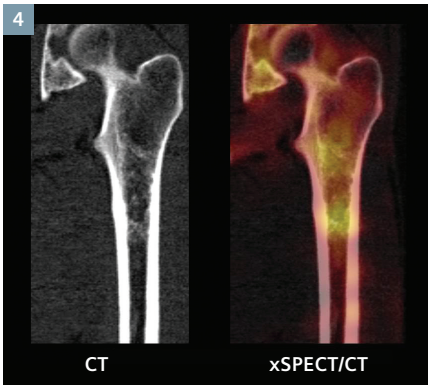

4 CT of the upper femoral shaft and lesser trochanter show mild sclerosis within the marrow, along with slight cortical thickening that corresponded to the focal hot area in the shaft. There was also diffuse sclerosis at the level of lesser trochanter with corresponding mild hypermetabolism with a translucent zone in between.

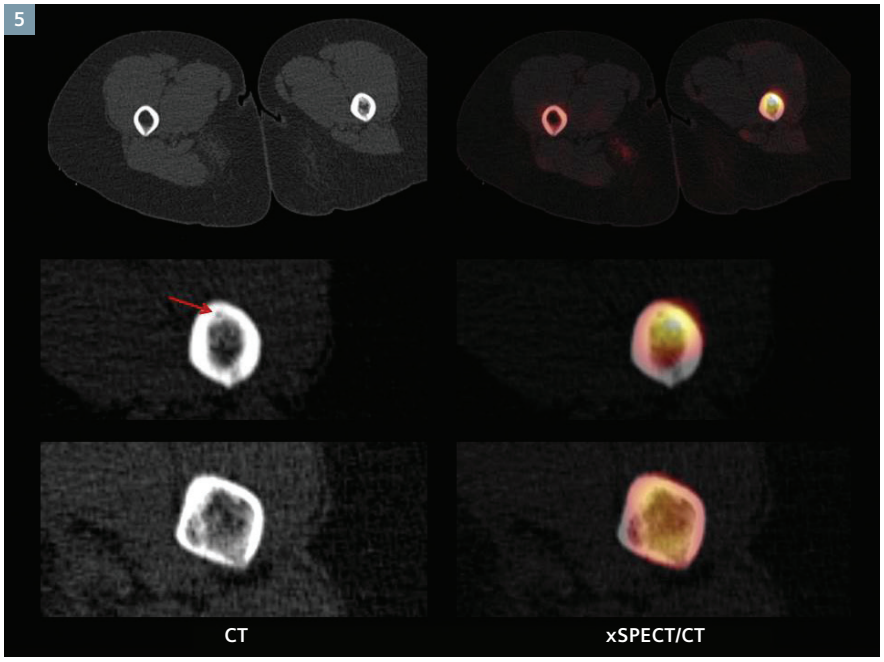

5 Axial CT and fused images through the region of maximum uptake intensity and section just above show marrow sclerosis and inner cortical irregularity along with cortical thickening that corresponded to the skeletal hypermetabolism. There was a small focal hypo-intense area in the anterior cortex (*red arrow*) that appeared to be a nidus related to Osteoid Osteoma.

with the area of diffuse sclerosis involving the anterior part of the marrow. There was a small focal hypo-intense area within the anterior cortex at the same level that had the appearance of the nidus of Osteoid Osteoma. The region of mild uptake in the marrow at the level of lesser trochanter was also associated with variegated sclerosis within the trabeculae, along with irregularity in the inner cortex.

Comments

The CT visualization of diffuse variegated sclerosis in the marrow and cortical thickening that corresponded to the area of maximum skeletal hypermetabolism, along with the focal hypointense area in the anterior cortex with the appearance of a nidus, was strongly suggestive of an Osteoid Osteoma. The diffuse sclerosis was a reactive change around the nidus, as is typically seen in Osteoid Osteoma. The intensity of skeletal hypermetabolism was a reflection of the diffuse sclerosis. The region of maximum hypermetabolism in the femoral shaft corresponded to the region of the nidus. At the lesser trochanteric level, a lower level of hypermetabolism was in the surrounding reactive sclerosis in the region above the nidus.

Conclusion

xSPECT Bone sharply defined the increased uptake to the upper femoral shaft, involving the anterior and lateral part of the cortex and adjacent marrow, aiding diagnostic confidence. Such clarity in distribution of skeletal metabolism could potentially improve evaluation of small bone and joint lesions.

Examination Protocol

Scanner	Symbia Intevo 16
Injected Dose	20 mCi of ^{99m}Tc MDP
Scan Protocol	SPECT: 32 stops, 20 sec/stop CT: 130 kV 50 mAs; slice collimation, 16x2.5 mm; slice thickness, 3 mm

* Symbia Intevo and xSPECT Bone are not commercially available in all countries. Due to regulatory reasons their future availability cannot be guaranteed. Please contact your local Siemens organization for further details.

Reversible Anteroseptal Ischemia Detected by Stress-rest Myocardial Perfusion using IQ•SPECT

By **Antonio Garcia, MD, Department of Nuclear Medicine**

Data courtesy of Manila Doctors Hospital, Manila, Philippines

History

A 65-year-old man with a long-standing history of diabetes presented with progressively increasing shortness of breath during exertion and occasional chest pain. The patient was referred for a stress-rest ^{99m}Tc MIBI myocardial perfusion study. The study was performed on a Symbia Intevo™* 16 xSPECT* (integrated SPECT and CT) system, using IQ•SPECT for fast cardiac SPECT acquisition. Prior to the study, the patient underwent exercise on a treadmill. The exercise had to be terminated due to breathlessness and significant ST depression. At the highest exercise level achieved, 15 mCi ^{99m}Tc MIBI was injected. The IQ•SPECT study was performed 30 minutes following the injection. A low-dose CT was acquired for attenuation correction (AC). The stress IQ•SPECT study was performed using a variable zoom collimator and a cardio-centric orbit, which help ensure the heart consistently remains at the center of orbit. This achieves higher count rates, and thus enables a four-minute SPECT acquisition. Following the supine stress, IQ•SPECT study, the patient was placed in the prone position. Then the IQ•SPECT study was repeated with the detector position altered to accommodate the prone positioning. Study parameters for the prone acquisition were the same as the supine (17 views at 13 sec/view). The stress IQ•SPECT acquisition was completed within 5 minutes. The prone acquisition was performed to compare with the supine study, with and without AC in order to ascertain the extent of AC.

Diagnosis

The stress study showed severe septal and apical hypoperfusion, both in supine, prone non-AC and supine CT attenuation-corrected images (*Figure 1*). Inferior wall attenuation effects were pronounced in the supine non-AC images. The prone images showed slight improvement, and the CT attenuation correction (CTAC) for the supine images showed significant improvement in the inferior wall uptake, demonstrating the extent of attenuation. The lateral wall showed the best preserved uptake in the stress images. There was considerable left ventricular dilatation following stress, which is reflective of severe ischemia secondary to advanced and multi-vessel coronary artery disease.

The rest study was acquired after 3 hours following a 3.5 mCi IV injection of Thallium. The rest study was acquired in the supine position, following a low-dose CT for AC. IQ•SPECT acquisition was used, and the duration of the acquisition was slightly longer than that of the stress study.

The rest study (*Figure 2,* pg. 28) showed considerably improved uptake in the apex and septum, which were grossly hypo-perfused in the stress study, suggesting significant myocardial reversibility in the grossly ischemic left anterior descending (LAD) territory. There was considerable attenuation effects in the uncorrected resting images in the inferior wall, posterior part of septum and posterobasal wall, of which showed significant improvement following CTAC. The left ventricle (LV) cavity size in the resting images appeared normal, considering the significant post-stress dilation visualized in the stress study.

1

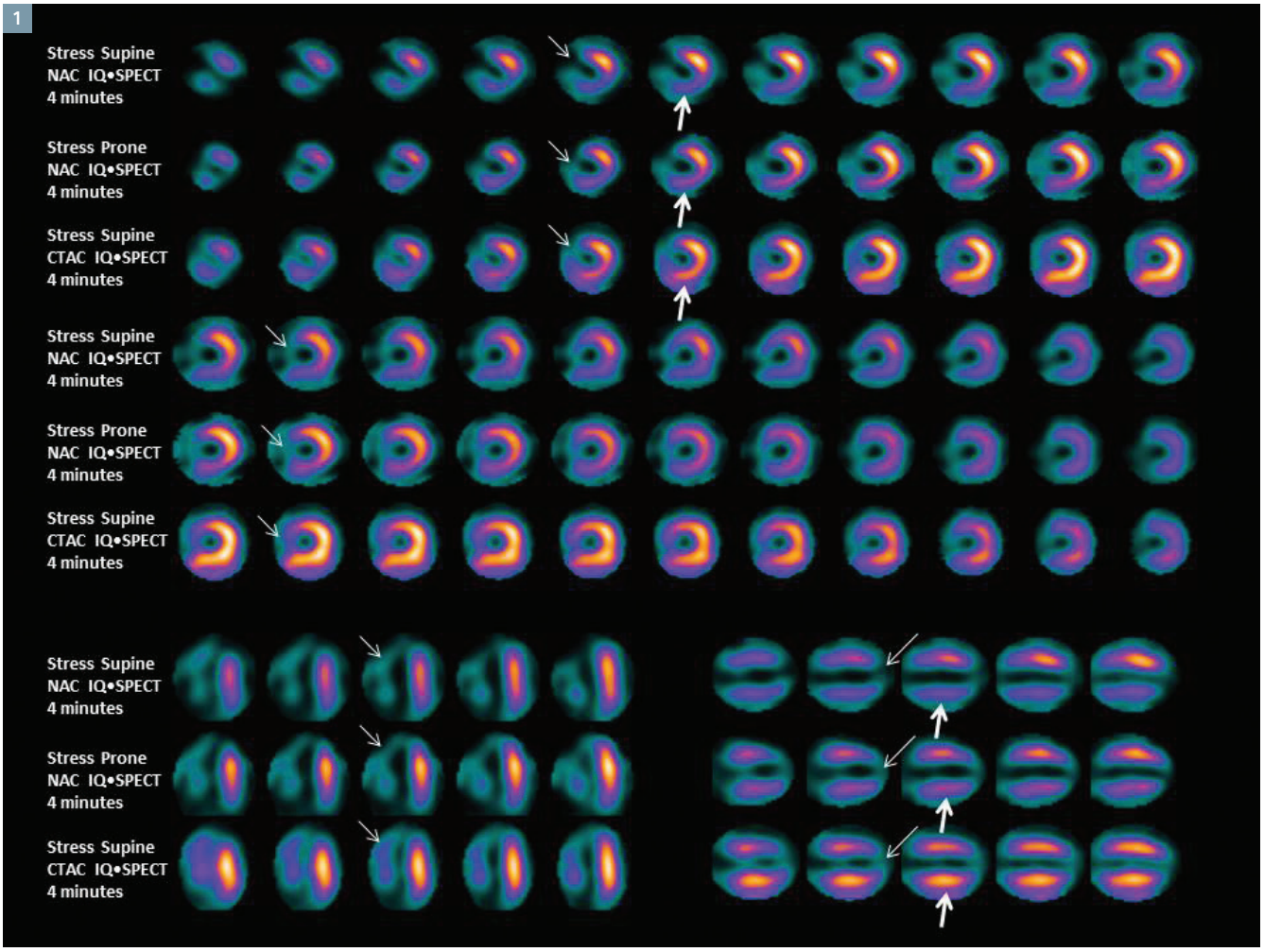

1 Comparison of stress supine non-AC, prone non-AC and supine with CTAC shows large and severe stress perfusion defects in the septum and apex (*arrow*). The inferior wall shows decreased uptake in the supine non-AC images, while the uptake slightly improved in the prone images even without AC. There was considerable improvement of the inferior wall uptake in the supine images, with CTAC confirming the presence of considerable inferior wall attenuation (*thick arrows*).

2

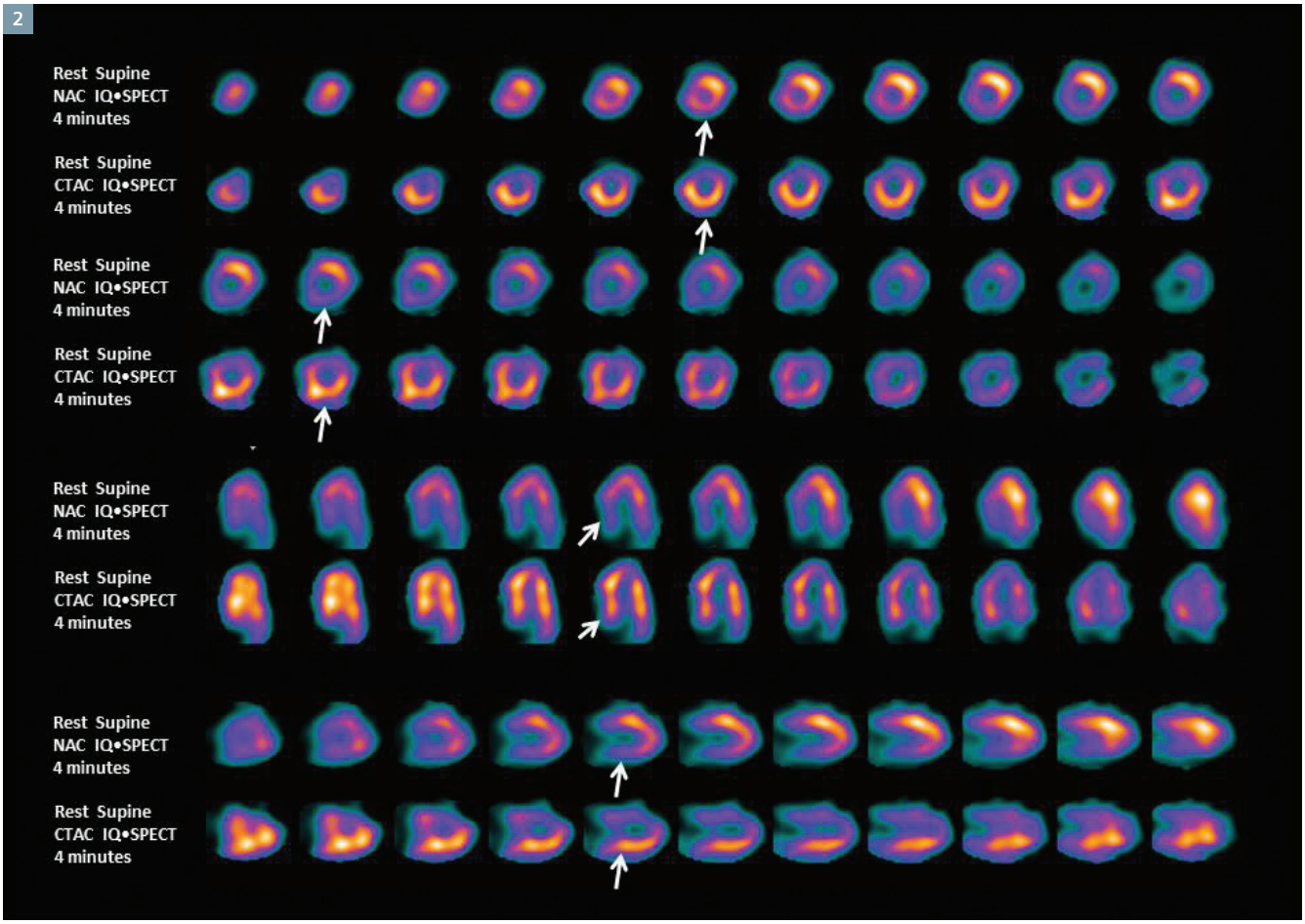

2 Comparison of supine, non-AC, rest study with the same data following AC shows considerable tracer uptake throughout the left ventricle, especially in the apex and septum. This suggested myocardial reversibility. In the uncorrected images, there was considerable attenuation in the inferior wall, showing significant increased uptake in the CTAC images (*arrows*). There was slightly decreased uptake in the anterior wall in the CTAC images, which was related to re-normalization following the correction of the inferior wall attenuation effect. The posterior part of the septum and the posterobasal wall also showed significant attenuation effect, which is corrected with CTAC (*arrows*).

Comments

Stress ^{99m}Tc MIBI and rest Tl-201 myocardial perfusion SPECT•CT study with IQ•SPECT clearly demonstrated a severe but completely reversible perfusion defect in the apex and adjacent anterior wall, septum and inferoapical segment—all of which suggested severe but reversible ischemia in the LAD territory. The significant post-stress LV dilatation suggested advanced coronary artery disease, most likely to be multivessel disease, although the LAD territory was the most severely affected. The complete reversibility of the entire ischemic zone suggested a possibility of complete restoration of myocardial contractility following revascularization.

The prone acquisition without AC when compared to supine non-AC images demonstrated considerable improvement in the inferior wall uptake, due to reduction of the attenuation effect obtained with prone imaging. When prone images were compared to supine CTAC images, the uptake in the inferior and posterobasal walls were comparable, since both prone and supine CTAC images showed reduction of attenuation effects. However, the degree of AC was far higher with CTAC on the supine images than what was obtained with prone non-CTAC images.

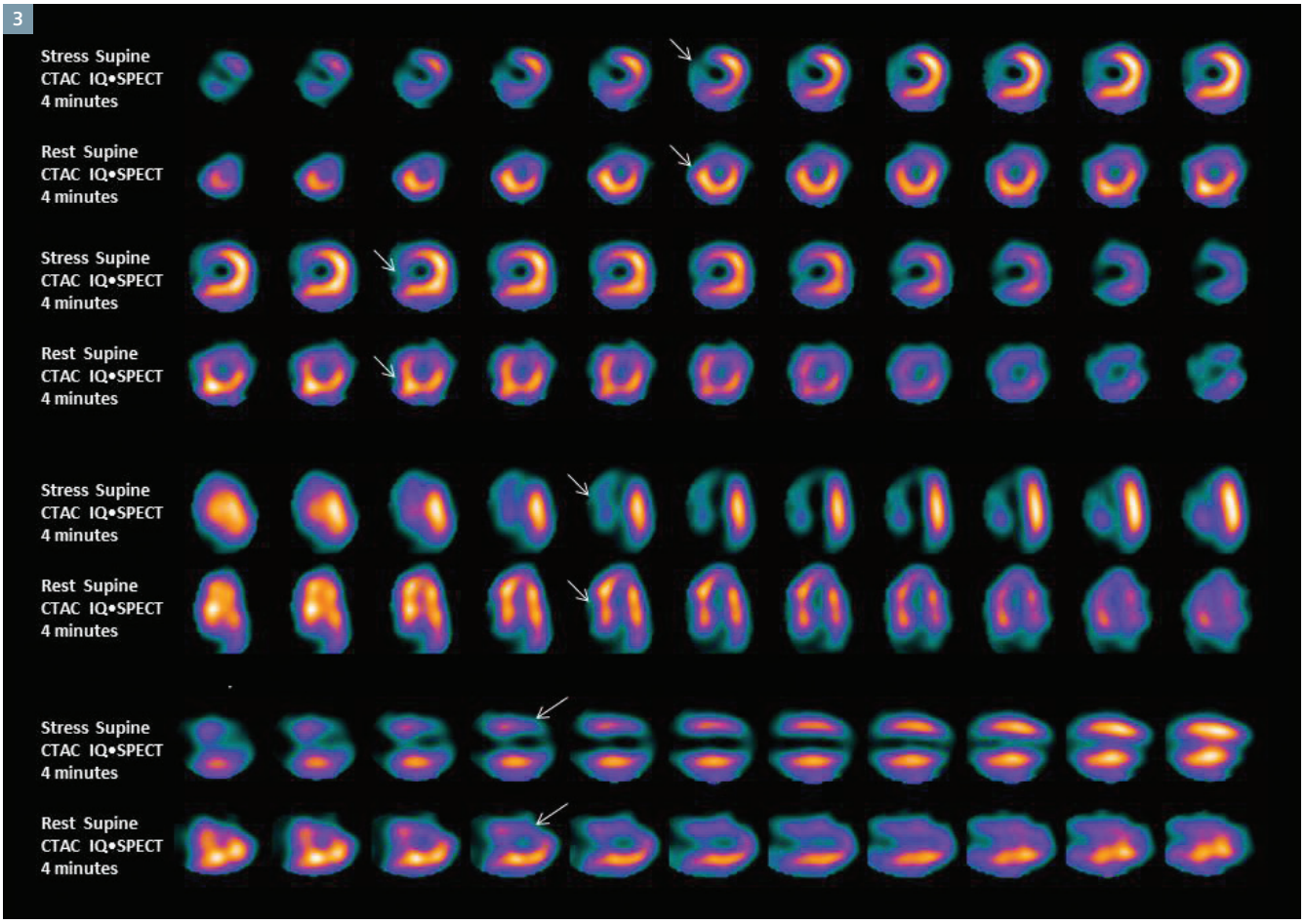

3 Supine CTAC stress and rest myocardial perfusion SPECT images show gross ischemia in the apex and septum (LAD territory) as well as an inferoapical segment with complete reversibility seen in the resting images. This suggested severe but reversible ischemia in the LAD territory.

Conclusion

IQ•SPECT enables fast cardiac acquisition (5 minutes) with CTAC, which, in this case, helped improve the attenuation effects seen in the inferior wall and posterobasal segments.

Examination Protocol

Scanner	Symbia Intevo 16 with IQ•SPECT
Injected Dose	Stress, 15 mCi of ^{99m}Tc MIBI; rest, 3.5 mCi of Thallium 201
Scan Delay	30 min post injection
Stress	CT: 130 kV 26 mAs; 16x1.2 mm collimation; IQ•SPECT, 17 views 13 sec/view
Rest	CT: 130 kV 26 mAs; 16x1.2 mm collimation IQ•SPECT, 17 views 18 sec/view

* Symbia Intevo is not commercially available in all countries. Due to regulatory reasons its future availability cannot be guaranteed. Please contact your local Siemens organization for further details.

The statements by Siemens customers described herein are based on results that were achieved in the customer's unique setting. Since there is no "typical" hospital and many variables exists (e.g., hospital size, case mix, level of IT adoption) there can be no guarantee that other customers will achieve the same results.

Pre-operative Assessment of Lung Perfusion using ^{99m}Tc MAA SPECT•CT in a Case of Epidermal Naevus Syndrome with Hemi-Dysplasia

By Dale L. Bailey, PhD, Kathy P. Willowson, PhD, Denis Gradinscak, MB, BS, FRANZCR, and Paul J. Roach, MB, BS, FRACP

Data courtesy of the Department of Nuclear Medicine, Royal North Shore Hospital and Institute of Medical Physics, University of Sydney, Sydney, Australia

History

An 18-year-old male with epidermal naevus syndrome and hemi-dysplasia presented with recent haemoptysis that was thought to be originating from a hypoplastic right lung—particularly the right lower lobe—based on CT and bronchoscopy findings. A request was made to evaluate the patient's lung ventilation and perfusion with SPECT/CT V/Q prior to possible right lower lobectomy.

A V/Q lung scan was performed on a Symbia™ T16 SPECT•CT. The ventilation scan was performed after the subject inhaled approximately 40 MBq of ^{99m}Tc Technegas. The perfusion scan followed the ventilation scan after the IV administration of 226 MBq ^{99m}Tc MAA. The only difference to a conventional V/Q scan (mainly for the investigation of pulmonary embolus) was that the ventilation and perfusion agents were administered with the subject in the upright position, rather than supine. This was done to better match the imaging findings to those obtained with conventional pulmonary function tests. Both data sets were acquired with LEHR collimators. Following the conventional planar images, a SPECT•CT study was performed for both ventilation and perfusion studies. The acquisition time per projection was 12 seconds for ventilation and 8 seconds for perfusion. 30 projections per detector (60 in total) were acquired at 3° radial increments using continuous acquisition motion. The count rate in the posterior projection was measured for ventilation (1.8 kcps) and after the perfusion radiopharmaceutical was administered (8.5 kcps), to ensure minimal contribution from the Technegas into the perfusion scan. The ventilation-corrected ratio of the Q:V count rates was 3.7:1. The aim was to have the ratio of perfusion radioactivity to ventilation radioactivity of no less than 3-4:1. A low-dose CT scan without contrast enhancement was acquired contemporaneously with the subject breathing freely.

The images were reconstructed with correction for scatter and attenuation based on the CT scan (*Figure 1*). The ventilation component in the reconstructed perfusion images was corrected by subtracting the co-registered ventilation images from the perfusion images after allowing for decay and the difference in acquisition time between the two studies. The CT scan was segmented manually by an experienced operator with guidance from a radiologist. 5 regions of interest (ROI) were defined on the transverse slices of the CT scan that corresponded to the 5 anatomical lobes of the lungs: left upper (LUL) and lower lobes (LLL), right upper (RUL), middle (RML) and lower (RLL) lobes. These lobar ROIs were then used to derive the total radioactivity (as reconstructed counts) per lobe for both the ventilation and perfusion scans.

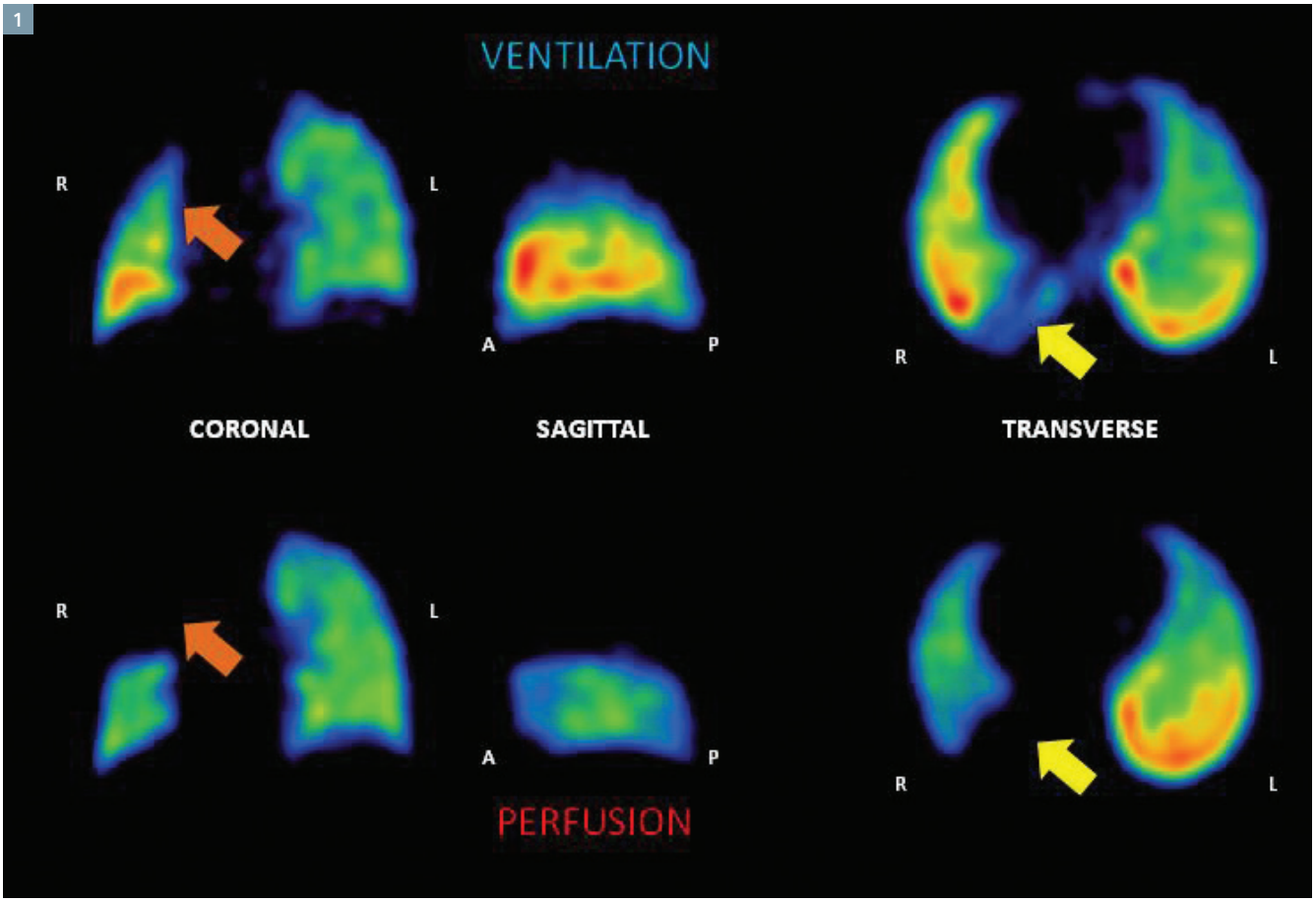

1 Representative SPECT V:Q images in the transverse, coronal and sagittal planes. The orange arrows indicate a large segmental region in the RUL, which was ventilated but not perfused, while the yellow arrows indicate an area of reduced ventilation and absent perfusion in the lower lobe of the right lung.

2

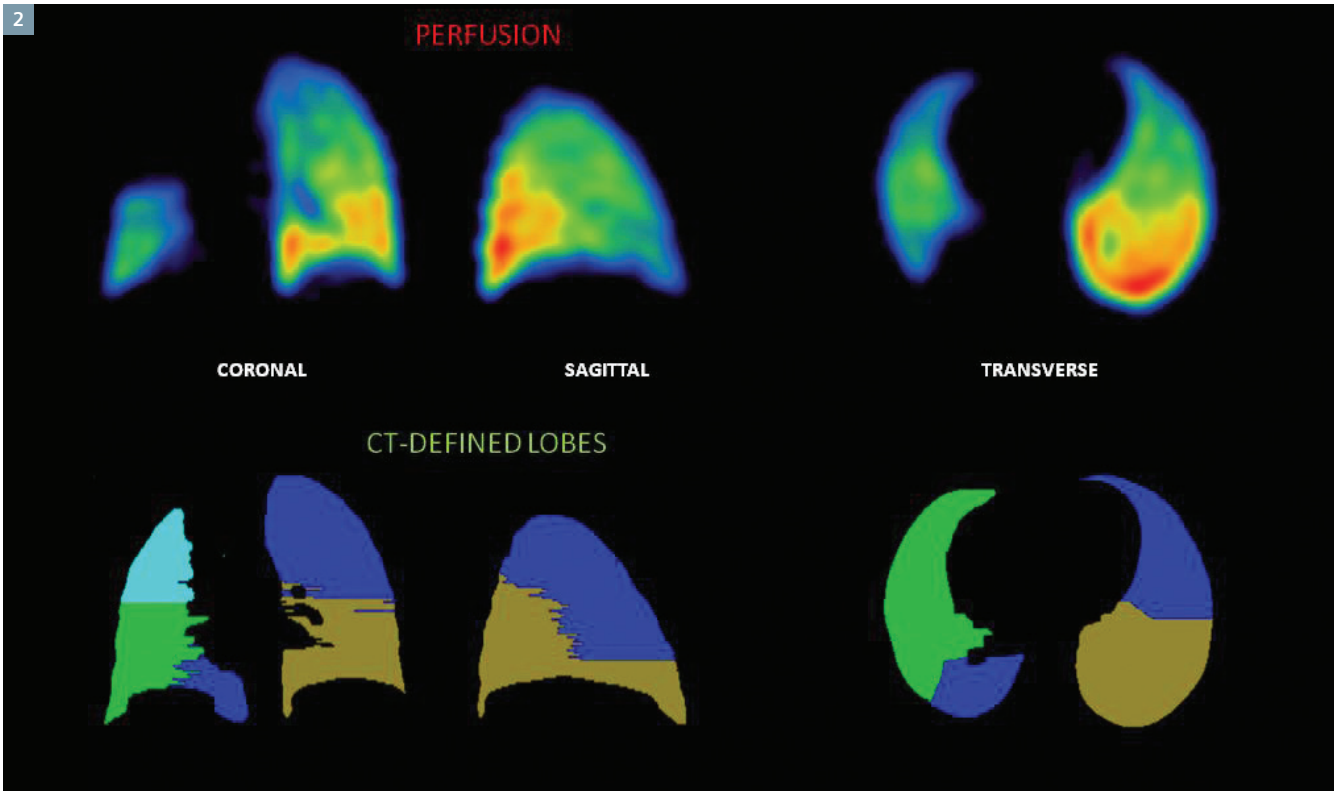

2 The segmented lobes on the CT scans are shown along with the co-registered perfusion SPECT images.

Diagnosis

Sample images for the ventilation and perfusion scans are shown in *Figure 1*. The lack of perfusion to the RUL seen in *Figure 1* was an unexpected finding and is probably due to congenital malformation of the pulmonary arterial vasculature with relatively normal bronchial development.

The CT-defined lobes are shown in *Figure 2*, along with the co-registered perfusion scan.

The CT-component of the SPECT•CT scan allows the anatomical volumes to be measured, as well as the functional V and Q contribution of each lobe. In this case, the contributions are shown in Table 1.

Lobe	Volume (%)	Ventilation (%)	Perfusion (%)
LLL	24.6	28.5	39.9
RLL	7.3	5.3	0.5
LUL	37.6	36.8	45.3
RML	19.8	23.0	13.3
RUL	10.8	6.3	0.9

Table 1: Anatomical and functional contributions as a percentage of the total lung.

Seen in *Figure 2*, the RML, at 19.8% by volume, was much larger than in a normal adult where it accounts for approximately 10% or less of total lung volume. In addition, the RLL was small at 7.3% where it would normally be contributing 20% of overall lung volume. On the functional studies, while the RUL and RLL were ventilated (6.3% and 5.3% respectively), they are hardly perfused at all (0.9% and 0.5%). Split lung function was 65.4% (ventilation) and 85.3% (perfusion) for the left lung, and 34.6% (ventilation) with 14.7% (perfusion) for the right lung. The perfusion of the right lung was almost totally contributed by the enlarged RML.

Comments

Epidermal Nevus Syndrome is a rare skin condition related to ichthyosis. The term epidermal nevus is a term applied to a variety of congenital skin lesions characterized by raised, thickened patches of skin or rough yellow-brown lesions, sometimes accompanied by erythema. Epidermal nevi may be small and solitary; it may be widespread but confined to one side of the body; or it may be widespread and covering both sides of the body. In this case, though, the presenting problem was refractory haemotpysis, and lobectomy was under consideration as a treatment.

The SPECT•CT V/Q scan was undertaken to assess the contribution to overall lung function of the RLL that had previously been identified as the source of the haemoptysis. While the RLL was still being ventilated (5.3% of overall ventilation), almost contributing proportionately based on its volume (7.3%), there was little perfusion. As such, gas exchange was negligible. More surprising, however, was that the RUL was also very poorly perfused. The right lung's contribution to total perfusion was about 15%, suggesting that even if the subject were to undergo a pneumonectomy, if required, it would not have a large impact on pulmonary function. The subject subsequently underwent a bronchial artery embolization of the RLL.

Conclusion

SPECT V/Q imaging provided unique information about regional pulmonary ventilation and perfusion. Combining the investigation with CT helped define lobar ROIs, which also enabled anatomical volumes to be derived. When combined with laboratory-based conventional pulmonary function tests, the study provided a comprehensive assessment of regional lung function.

Examination Protocol

Scanner	Symbia T16
Injected Dose	Ventilation scan, 40 MBq of ^{99m}Tc Technegas; perfusion scan, 226 MBq ^{99m}Tc MAA
Parameters	64 frames, 15 sec/frame; 3D OSEM reconstruction

References:
1. **Willowson K, Bailey DL, Baldock C.** "Quantitative SPECT Reconstruction Using CT-Derived Corrections." *Phys Med Biol.* 2008, 53: 3099-3112.

SPECT/CT for Patient-specific Dosimetry in Radionuclide Therapy

By **Jean-Mathieu Beauregard, MD, MSc, FRCPC, Université Laval, Quebec City, Quebec, Canada**

Data courtesy of Peter MacCallum Cancer Centre, Melbourne, Australia

In nuclear medicine, dosimetry has 2 main purposes. First, dosimetry can be performed with the goal of determining the average radiation exposure during a particular nuclear medicine procedure. Radiopharmaceutical uptake and kinetics data are then gathered in cohorts and applied to a given model (e.g., "adult male" or "adult female" in Olinda/MIRD software) to yield radiation exposure per unit of administered activity (e.g., mSv/MBq) for specific organs and the whole body. The latter value, called the "effective dose," is used as an index of the theoretical radiation-related risk of the procedure for the general population, and allows comparison of this risk to that of other diagnostic imaging procedures. Secondly, dosimetry can be performed in individual patients with the goal of accurately determining the radiation doses absorbed in organs and tumors before or during radionuclide therapy. This, in turn, allows assessing or predicting therapeutic efficacy and toxicity, and ultimately personalizing radionuclide therapy. In this setting, average exposure values from cohort studies extrapolated to the individual patient have a limited utility because of the large inter-individual variability in factors affecting the biodistribution.

Traditionally, clinical dosimetry studies for single photon-emitting radiopharmaceuticals, including beta particle-emitting therapeutic agents, have been performed using serial planar scintigraphy. However, the accuracy of planar scintigraphy for activity quantitation is limited by many factors. First, tissue superimposition requires background activity subtraction, which is performed by placing a

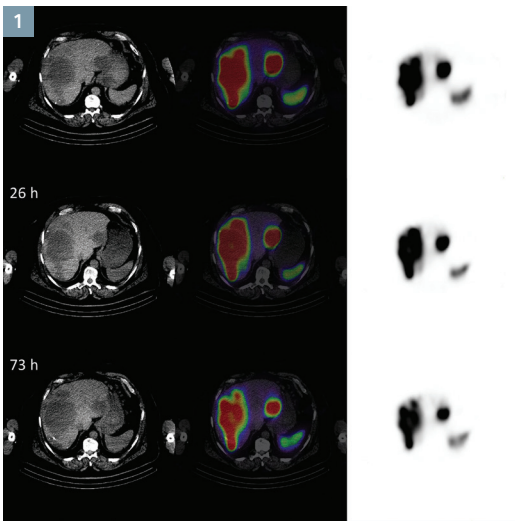

1 A patient with a metastatic mid-gut carcinoid tumor was scanned at 3 time points following the administration of 7.4 GBq of a ^{177}Lu-based radiopharmaceutical. Corresponding transaxial SPECT/CT slices were presented (from left to right: CT, fusion and SPECT). There was very high uptake in hepatic metastases, which were hypodense on non-contrast, low-dose CT. The uptake in the spleen was moderate. Resulting absorbed radiation doses were 22.4 Gy and 6.5 Gy, respectively, for the tumor and spleen.

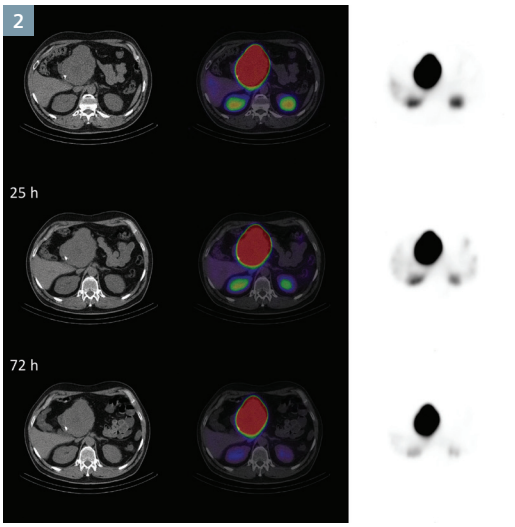

2 Another patient with inoperable localized pancreatic neuroendocrine tumor underwent serial SPECT/CT following the administration of 8.0 GBq of a ^{177}Lu-based radiopharmaceutical. The uptake was much higher in the primary tumor mass in the pancreatic head than it was in the kidneys. Moreover, the kidneys exhibited a faster clearance of activity over time. The resulting absorbed radiation doses were 35.3 Gy and 2.9 Gy, respectively, for the tumor and kidney.

background region of interest (ROI) close to the organ or tumor ROI. While background is assumed to be uniform in the area, it may not always be the case. The situation is more complex when more than one structure with significant uptake are superimposed together and inseparable on a 2D scintigraphy. SPECT/CT overcomes these limitations by providing the ability to draw 3D volumes of interest (VOI) over organs and lesions, without the need for background subtraction and without tissue superimposition. The CT component allows precise separation of the tissues of interest from other structures and refines VOIs accordingly.

To determine the energy deposited locally from radiation, the concentration of activity must be known at multiple time points. While planar scintigraphy can be used to estimate the total activity of an organ, it is not accurate for measuring the volume of that organ to calculate the activity concentration. Again, SPECT/CT solves this problem, as both total activity and volume of organs can be resolved from SPECT and CT components, respectively. Moreover, in larger structures, the activity concentration can be directly sampled using a small spherical VOI placed over an area of uniform uptake.

Similar to PET, accurate activity quantitation in single-photon imaging requires attenuation correction. Attenuation correction is not readily available for planar imaging. When a standard source is placed in the field of view during a planar acquisition, its attenuation may not be the same as the structure of interest within the subject's body. Conversely, attenuation correction comes standard with SPECT/CT systems, such as the Symbia™ T Series. This makes it possible to calibrate the camera with sources of a particular radionuclide. SPECT reconstruction with attenuation correction will then allow activity concentration to be resolved more accurately than planar imaging techniques in patients of different sizes. Scatter correction, also implemented on Symbia T systems, further enhances image quality and quantitation accuracy, while resolution recovery with the 3D iterative reconstruction algorithm improves resolution, thus decreasing partial volume effect for smaller structures.

While planar imaging-based dosimetry allows application of conventional model-based dosimetry (e.g., Olinda/MIRD), SPECT/CT opens the pathway to newer techniques that are truly patient-specific, such as full 3D voxel dosimetry. Axial acquisition length is not limited since multiple-bed-position SPECT/CT acquisition is now possible. Planar scintigraphy may be faster to acquire, but modern camera systems such as Symbia have improved counting sensitivity and reconstruction algorithms. This means that SPECT/CT acquisition times can be shortened significantly while maintaining image quality, thus making the use of SPECT/CT more convenient and appealing than ever before. By carefully selecting the most relevant scanning time points, it is possible to develop 3D dosimetry protocols that are practical enough to be integrated into routine clinical practice. In a radionuclide therapy setting, additional radiation exposure from the CT component of SPECT/CT is negligible when compared with the therapeutic radiation dose, particularly when the CT scan is performed at low or very low dose.

SPECT/CT fusion visualization and analysis software is an essential component of a SPECT/CT-based dosimetry system. An application allowing automatic registration of multiple-time-point SPECT/CT studies, such as TrueD™, greatly simplifies analysis by allowing a VOI to be drawn on all time points at once and by outputting uptake data in a convenient format, ready for calculation of residence times and absorbed radiation dose values.

At the Centre for Cancer Imaging at Peter MacCallum Cancer Centre (Melbourne, Australia), SPECT/CT dosimetry is performed for patients suffering from neuroendocrine tumor undergoing ^{177}Lu-based radiopharmaceutical therapy*. ^{177}Lu radionuclide is particularly well suited for dosimetry studies, because of its moderate abundance of medium-energy gamma photons (main ^{177}Lu photopeak: 208 keV, 11% abundance). Indeed, for target tissues with high uptake, there is very little contribution to the absorbed dose from gamma decay occurring elsewhere in the body. The Centre's state-of-the-art Symbia T6 SPECT/CT system, fitted with medium-energy, low-penetration collimators, has been calibrated using ^{177}Lu sources having a wide range of activity. The SPECT data is reconstructed using the system's iterative algorithm with CT-based attenuation correction, scatter correction and Flash 3D resolution recovery. Additionally, dead-time correction is performed using a custom *syngo*® MI Apps workflow.[1] This clinical dosimetry protocol includes whole-body SPECT/CT scanning at 3 time points (*Figures 1* and *2*). Activity concentration is sampled using small VOIs and data is plotted to define time-activity curves, allowing determination of absorbed radiation doses from local decay.

Because each patient is different, there is a need to tailor radionuclide therapy so that maximum therapeutic efficacy can be achieved with minimum toxicity. Such an approach fully embraces the principles of personalized medicine. SPECT/CT dosimetry offers clear advantages over traditional dosimetry techniques in terms of accuracy and specificity to individual patients, and is a promising tool to allow personalized radionuclide therapy to expand in the near future.

References:

1. **Beauregard et al.** *Cancer Imaging.* 2011, 11: 56-66.

* The concepts and information presented are still under development and are not commercially available yet. Their future availability cannot be ensured.

Siemens Healthcare
Customer Magazines

Our customer magazine family offers the latest information and background for every healthcare field. From the hospital director to the radiological assistant—here, you can quickly find information relevant to your needs.

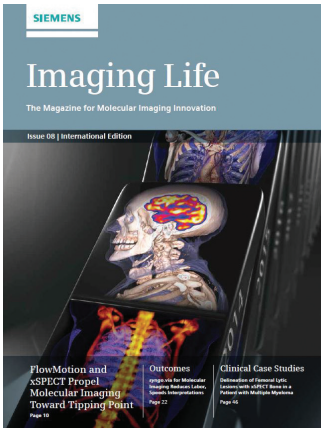

Imaging Life
Everything from the world of molecular imaging innovations.

AXIOM Innovations
Everything from the world of interventional radiology, cardiology, and surgery.

Medical Solutions
Innovations and trends in healthcare. The magazine is designed especially for members of hospital management, administration personnel and heads of medical departments.

Scan and Subscribe!

For current and past issues and to order the magazines, please visit **www.siemens.com/healthcare-magazine**

MAGNETOM Flash
Everything from the world of magnetic resonance imaging.

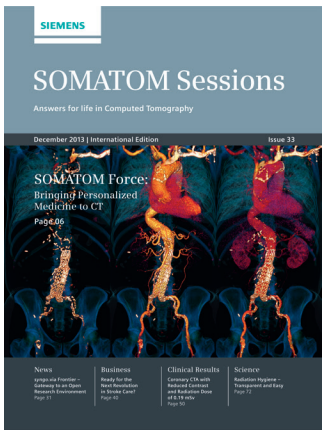

SOMATOM Sessions
Everything from the world of computed tomography.

There's an Imaging Life App! Download the *Imaging Life* app to read the magazine on your mobile device. You can also read the magazine online at: **www.siemens.com/imaginglife**

Publisher:
Siemens Medical Solutions USA, Inc.
Healthcare Sector Molecular Imaging
2501 N. Barrington Road
Hoffman Estates, IL 60192
USA
Telephone: + 1 847 304-7700
www.siemens.com/mi

Editor: Rhett Morici
rhett.morici@siemens.com

Responsible for Content:
Partha Ghosh
partha.ghosh@siemens.com

Design Consulting:
VieceliDesign, Inc., Utah, USA

Printer: Tewell Warren Printing,
Colorado, USA

Note in accordance with § 33 Para.1 of the German Federal Data Protection Law: Dispatch is made using an address file which is maintained with the aid of an automated data processing system.

We remind our readers that when printed, X-ray films never disclose all the information content of the original. Artifacts in CT, MR, SPECT, SPECT/CT, PET, PET/CT and PET/MR images are recognizable by their typical features and are generally distinguishable from existing pathology. As referenced below, healthcare practioners are expected to utilize their own learning, training and expertise in evaluating images.

Please contact your local Siemens sales representative for the most current information.

Note: Original images always lose a certain amount of detail when reproduced. All comparative claims derived from competitive data at the time of printing. Data on file.

The consent of the authors and publisher are required for the reprint or reuse of an article. Please contact Siemens for further information. Suggestions, proposals and information are always welcome; they are carefully examined and submitted to the editorial board for attention. Imaging Life is not responsible for loss, damage or any other injury to unsolicited manuscripts or materials.

We welcome your questions and comments about the editorial content of Imaging Life. Please contact us at imaginglife.healthcare@siemens.com.

Imaging Life is available on the internet: www.siemens.com/imaginglife

Imaging Life also has a free iPad and iPhone App available. From your iPad or iPhone, go to the App Store and search "Imaging Life," then download.

Some of the imaging biomarkers in this publication are not currently recognized by the U.S. Food and Drug Administration (FDA) or other regulatory agencies as being safe and effective, and Siemens does not make any claims regarding their use.

Clinical Images Courtesy of:

Pg. 4-7 University of Tennessee, Knoxville, TN, USA;

Pg. 8-9 Medical University of Hannover, Hannover, Germany;

Pg. 10-11 Rigshospitalet, Copenhagen, Denmark;

Pg. 12-13 Hospital University of Geneva, Geneva, Switzerland;

Pg. 14-17 Bad Berka Zentralklinic, Bad Berka, Germany;

Pg. 18-21 Ludwig-Maximilians University, Munich, Germany

Pg. 22-23 Department of Nuclear Medicine, University of Erlangen, Erlangen, Germany;

Pg. 24-29 Manila Doctors Hospital, Manila, Philippines;

Pg. 30-33 Department of Nuclear Medicine, Royal North Shore Hospital and Institute of Medical Physics, University of Sydney, Sydney, Australia;

Pg. 34-35 Peter MacCallum Cancer Centre, Melbourne, Australia

HIGHLIGHTS OF PRESCRIBING INFORMATION

These highlights do not include all the information needed to use Fludeoxyglucose F 18 Injection safely and effectively. See full prescribing information for Fludeoxyglucose F 18 Injection.

Fludeoxyglucose F 18 Injection, USP

For intravenous use

Initial U.S. Approval: 2005

RECENT MAJOR CHANGES

Warnings and Precautions (5.1, 5.2) 7/2010

Adverse Reactions (6) 7/2010

INDICATIONS AND USAGE

Fludeoxyglucose F18 Injection is indicated for positron emission tomography (PET) imaging in the following settings:

- Oncology: For assessment of abnormal glucose metabolism to assist in the evaluation of malignancy in patients with known or suspected abnormalities found by other testing modalities, or in patients with an existing diagnosis of cancer.
- Cardiology: For the identification of left ventricular myocardium with residual glucose metabolism and reversible loss of systolic function in patients with coronary artery disease and left ventricular dysfunction, when used together with myocardial perfusion imaging.
- Neurology: For the identification of regions of abnormal glucose metabolism associated with foci of epileptic seizures (1).

DOSAGE AND ADMINISTRATION

Fludeoxyglucose F 18 Injection emits radiation. Use procedures to minimize radiation exposure. Screen for blood glucose abnormalities.

- In the oncology and neurology settings, instruct patients to fast for 4 to 6 hours prior to the drug's injection. Consider medical therapy and laboratory testing to assure at least two days of normoglycemia prior to the drug's administration (5.2).
- In the cardiology setting, administration of glucose-containing food or liquids (e.g., 50 to 75 grams) prior to the drug's injection facilitates localization of cardiac ischemia (2.3).

Aseptically withdraw Fludeoxyglucose F 18 Injection from its container and administer by intravenous injection (2).

The recommended dose:

- for adults is 5 to 10 mCi (185 to 370 MBq), in all indicated clinical settings (2.1).
- for pediatric patients is 2.6 mCi in the neurology setting (2.2).

Initiate imaging within 40 minutes following drug injection; acquire static emission images 30 to 100 minutes from time of injection (2).

DOSAGE FORMS AND STRENGTHS

Multi-dose 30mL and 50mL glass vial containing 0.74 to 7.40 GBq/mL (20 to 200 mCi/mL) Fludeoxyglucose

F 18 Injection and 4.5mg of sodium chloride with 0.1 to 0.5% w/w ethanol as a stabilizer (approximately 15 to 50 mL volume) for intravenous administration (3).

CONTRAINDICATIONS

None

WARNINGS AND PRECAUTIONS

- Radiation risks: use smallest dose necessary for imaging (5.1).
- Blood glucose adnormalities: may cause suboptimal imaging (5.2).

ADVERSE REACTIONS

Hypersensitivity reactions have occurred; have emergency resuscitation equipment and personnel immediately available (6).

To report SUSPECTED ADVERSE REACTIONS, contact PETNET Solutions, Inc. at 877-473-8638 or FDA at 1-800-FDA-1088 or www.fda.gov/medwatch.

USE IN SPECIFIC POPULATIONS

Pregnancy Category C: No human or animal data. Consider alternative diagnostics; use only if clearly needed (8.1).

- Nursing mothers: Use alternatives to breast feeding (e.g., stored breast milk or infant formula) for at least 10 half-lives of radioactive decay, if Fludeoxyglucose F 18 Injection is administered to a woman who is breast-feeding (8.3).
- Pediatric Use: Safety and effectiveness in pediatric patients have not been established in the oncology and cardiology settings (8.4).

See 17 for PATIENT COUNSELING INFORMATION

Revised: 1/2011

FULL PRESCRIBING INFORMATION: CONTENTS*

1 INDICATIONS AND USAGE
- 1.1 Oncology
- 1.2 Cardiology
- 1.3 Neurology

2 DOSAGE AND ADMINISTRATION
- 2.1 Recommended Dose for Adults
- 2.2 Recommended Dose for Pediatric Patients
- 2.3 Patient Preparation
- 2.4 Radiation Dosimetry
- 2.5 Radiation Safety – Drug Handling
- 2.6 Drug Preparation and Administration
- 2.7 Imaging Guidelines

3 DOSAGE FORMS AND STRENGTHS

4 CONTRAINDICATIONS

5 WARNINGS AND PRECAUTIONS
- 5.1 Radiation Risks
- 5.2 Blood Glucose Abnormalities

6 ADVERSE REACTIONS

7 DRUG INTERACTIONS

8 USE IN SPECIFIC POPULATIONS
- 8.1 Pregnancy
- 8.3 Nursing Mothers
- 8.4 Pediatric Use

11 DESCRIPTION
- 11.1 Chemical Characteristics
- 11.2 Physical Characteristics

12 CLINICAL PHARMACOLOGY
- 12.1 Mechanism of Action
- 12.2 Pharmacodynamics
- 12.3 Pharmacokinetics

13 NONCLINICAL TOXICOLOGY
- 13.1 Carcinogenesis, Muta-genesis, Impairment of Fertility

14 CLINICAL STUDIES
- 14.1 Oncology
- 14.2 Cardiology
- 14.3 Neurology

15 REFERENCES

16 HOW SUPPLIED/STORAGE AND DRUG HANDLING

17 PATIENT COUNSELING INFORMATION

* Sections or subsections omitted from the full prescribing information are not listed.

FULL PRESCRIBING INFORMATION

1 INDICATIONS AND USAGE

Fludeoxyglucose F 18 Injection is indicated for positron emission tomography (PET) imaging in the following settings:

1.1 Oncology

For assessment of abnormal glucose metabolism to assist in the evaluation of malignancy in patients with known or suspected abnormalities found by other testing modalities, or in patients with an existing diagnosis of cancer.

1.2 Cardiology

For the identification of left ventricular myocardium with residual glucose metabolism and reversible loss of systolic function in patients with coronary artery disease and left ventricular dysfunction, when used together with myocardial perfusion imaging.

1.3 Neurology

For the identification of regions of abnormal glucose metabolism associated with foci of epileptic seizures.

2 DOSAGE AND ADMINISTRATION

Fludeoxyglucose F 18 Injection emits radiation. Use procedures to minimize radiation exposure. Calculate the final dose from the end of synthesis (EOS) time using proper radioactive decay factors. Assay the final dose in a properly calibrated dose calibrator before administration to the patient [see Description (11.2)].

2.1 Recommended Dose for Adults

Within the oncology, cardiology and neurology settings, the recommended dose for adults is 5 to 10 mCi (185 to 370 MBq) as an intravenous injection.

2.2 Recommended Dose for Pediatric Patients

Within the neurology setting, the recommended dose for pediatric patients is 2.6 mCi, as an intravenous injection. The optimal dose adjustment on the basis of body size or weight has not been determined [see Use in Special Populations (8.4)].

2.3 Patient Preparation

- To minimize the radiation absorbed dose to the bladder, encourage adequate hydration. Encourage the patient to drink water or other fluids (as tolerated) in the 4 hours before their PET study.
- Encourage the patient to void as soon as the imaging study is completed and as often as possible thereafter for at least one hour.
- Screen patients for clinically significant blood glucose abnormalities by obtaining a history and/or laboratory tests [see Warnings and Precautions (5.2)]. Prior to Fludeoxyglucose F 18 PET imaging in the oncology and neurology settings, instruct patient to fast for 4 to 6 hours prior to the drug's injection.
- In the cardiology setting, administration of glucose-containing food or liquids (e.g., 50 to 75 grams) prior to Fludeoxyglucose F18 Injection facilitates localization of cardiac ischemia

2.4 Radiation Dosimetry

The estimated human absorbed radiation doses (rem/mCi) to a newborn (3.4 kg), 1-year old (9.8 kg), 5-year old (19 kg), 10-year old (32 kg), 15-year old (57 kg), and adult (70 kg) from intravenous administration of Fludeoxyglucose F 18 Injection are shown in Table 1. These estimates were calculated based on human[2] data and using the data published by the International Commission on Radiological Protection[4] for Fludeoxyglucose ^{18} F. The dosimetry data show that there are slight variations in absorbed radiation dose for various organs in each of the age groups. These dissimilarities in absorbed radiation dose are due to developmental age variations (e.g., organ size, location, and overall metabolic rate for each age group). The identified critical organs (in descending order) across all age groups evaluated are the urinary bladder, heart, pancreas, spleen, and lungs.

Table 1. Estimated Absorbed Radiation Doses (rem/mCi) After Intravenous Administration of Fludeoxyglucose F-18 Injection[a]

Organ	Newborn (3.4 kg)	1-year old (9.8 kg)	5-year old (19 kg)	10-year old (32 kg)	15-year old (57 kg)	Adult (70 kg)
Bladder wall[b]	4.3	1.7	0.93	0.60	0.40	0.32
Heart wall	2.4	1.2	0.70	0.44	0.29	0.22
Pancreas	2.2	0.68	0.33	0.25	0.13	0.096
Spleen	2.2	0.84	0.46	0.29	0.19	0.14
Lungs	0.96	0.38	0.20	0.13	0.092	0.064
Kidneys	0.81	0.34	0.19	0.13	0.089	0.074
Ovaries	0.80	0.8	0.19	0.11	0.058	0.053
Uterus	0.79	0.35	0.19	0.12	0.076	0.062
LLI wall *	0.69	0.28	0.15	0.097	0.060	0.051
Liver	0.69	0.31	0.17	0.11	0.076	0.058
Gallbladder wall	0.69	0.26	0.14	0.093	0.059	0.049
Small intestine	0.68	0.29	0.15	0.096	0.060	0.047
ULI wall **	0.67	0.27	0.15	0.090	0.057	0.046
Stomach wall	0.65	0.27	0.14	0.089	0.057	0.047
Adrenals	0.65	0.28	0.15	0.095	0.061	0.048
Testes	0.64	0.27	0.14	0.085	0.052	0.041
Red marrow	0.62	0.26	0.14	0.089	0.057	0.047
Thymus	0.61	0.26	0.14	0.086	0.056	0.044
Thyroid	0.61	0.26	0.13	0.080	0.049	0.039
Muscle	0.58	0.25	0.13	0.078	0.049	0.039
Bone surface	0.57	0.24	0.12	0.079	0.052	0.041
Breast	0.54	0.22	0.11	0.068	0.043	0.034
Skin	0.49	0.20	0.10	0.060	0.037	0.030
Brain	0.29	0.13	0.09	0.078	0.072	0.070
Other tissues	0.59	0.25	0.13	0.083	0.052	0.042

[a] MIRDOSE 2 software was used to calculate the radiation absorbed dose. Assumptions on the biodistribution based on data from Gallagher et al.1 and Jones et al.2

[b] The dynamic bladder model with a uniform voiding frequency of 1.5 hours was used. *LLI = lower large intestine; **ULI = upper large intestine

2.5 Radiation Safety – Drug Handling

- Use waterproof gloves, effective radiation shielding, and appropriate safety measures when handling Fludeoxyglucose F 18 Injection to avoid unnecessary radiation exposure to the patient, occupational workers, clinical personnel and other persons.
- Radiopharmaceuticals should be used by or under the control of physicians who are qualified by specific training and experience in the safe use and handling of radionuclides, and whose experience and training have been approved by the appropriate governmental agency authorized to license the use of radionuclides.
- Calculate the final dose from the end of synthesis (EOS) time using proper radioactive decay factors. Assay the final dose in a properly calibrated dose calibrator before administration to the patient [see Description (11.2)].
- The dose of Fludeoxyglucose F 18 used in a given patient should be minimized consistent with the objectives of the procedure, and the nature of the radiation detection devices employed.

2.6 Drug Preparation and Administration

- Calculate the necessary volume to administer based on calibration time and dose.
- Aseptically withdraw Fludeoxyglucose F 18 Injection from its container.
- Inspect Fludeoxyglucose F 18 Injection visually for particulate matter and discoloration before administration, whenever solution and container permit.
- Do not administer the drug if it contains particulate matter or discoloration; dispose of these unacceptable or unused preparations in a safe manner, in compliance with applicable regulations.
- Use Fludeoxyglucose F 18 Injection within 12 hours from the EOS.

2.7 Imaging Guidelines

- Initiate imaging within 40 minutes following Fludeoxyglucose F 18 Injection administration.
- Acquire static emission images 30 to 100 minutes from the time of injection.

3 DOSAGE FORMS AND STRENGTHS

Multiple-dose 30 mL and 50 mL glass vial containing 0.74 to 7.40 GBq/mL (20 to 200 mCi/mL) of Fludeoxyglucose F 18 Injection and 4.5 mg of sodium chloride with 0.1 to 0.5% w/w ethanol as a stabilizer (approximately 15 to 50 mL volume) for intravenous administration.

4 CONTRAINDICATIONS

None

5 WARNINGS AND PRECAUTIONS

5.1 Radiation Risks

Radiation-emitting products, including Fludeoxyglucose F 18 Injection, may increase the risk for cancer, especially in pediatric patients. Use the smallest dose necessary for imaging and ensure safe handling to protect the patient and health care worker [see Dosage and Administration (2.5)].

5.2 Blood Glucose Abnormalities

In the oncology and neurology setting, suboptimal imaging may occur in patients with inadequately regulated blood glucose levels. In these patients, consider medical therapy and laboratory testing to assure at least two days of normoglycemia prior to Fludeoxyglucose F 18 Injection administration.

6 ADVERSE REACTIONS

Hypersensitivity reactions with pruritus, edema and rash have been reported in the post-marketing setting. Have emergency resuscitation equipment and personnel immediately available.

7 DRUG INTERACTIONS

The possibility of interactions of Fludeoxyglucose F 18 Injection with other drugs taken by patients undergoing PET imaging has not been studied.

8 USE IN SPECIFIC POPULATIONS

8.1 Pregnancy

Pregnancy Category C

Animal reproduction studies have not been conducted with Fludeoxyglucose F 18 Injection. It is also not known whether Fludeoxyglucose F 18 Injection can cause fetal harm when administered to a pregnant woman or can affect reproduction capacity. Consider alternative diagnostic tests in a pregnant woman; administer Fludeoxyglucose F 18 Injection only if clearly needed.

8.3 Nursing Mothers

It is not known whether Fludeoxyglucose F 18 Injection is excreted in human milk. Consider alternative diagnostic tests in women who are breast-feeding. Use alternatives to breast feeding (e.g., stored breast milk or infant formula) for at least 10 half-lives of radioactive decay, if Fludeoxyglucose F 18 Injection is administered to a woman who is breast-feeding.

8.4 Pediatric Use

The safety and effectiveness of Fludeoxyglucose F 18 Injection in pediatric patients with epilepsy is established on the basis of studies in adult and pediatric patients. In pediatric patients with epilepsy, the recommended dose is 2.6 mCi. The optimal dose adjustment on the basis of body size or weight has not been determined. In the oncology or cardiology settings, the safety and effectiveness of Fludeoxyglucose F 18 Injection have not been established in pediatric patients.

11 DESCRIPTION

11.1 Chemical Characteristics

Fludeoxyglucose F 18 Injection is a positron emitting radiopharmaceutical that is used for diagnostic purposes in conjunction with positron emission tomography (PET) imaging. The active ingredient 2-deoxy-2-[^{18}F]fluoro-D-glucose has the molecular formula of $C_6H_{11}{}^{18}FO_5$ with a molecular weight of 181.26, and has the following chemical structure:

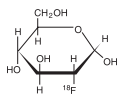

Fludeoxyglucose F 18 Injection is provided as a ready to use sterile, pyrogen free, clear, colorless solution. Each mL contains between 0.740 to 7.40GBq (20.0 to 200 mCi) of 2-deoxy-2-[^{18}F]fluoro-D-glucose at the EOS, 4.5 mg of sodium chloride and 0.1 to 0.5% w/w ethanol as a stabilizer. The pH of the solution is between 4.5 and 7.5. The solution is packaged in a multiple-dose glass vial and does not contain any preservative.

11.2 Physical Characteristics

Fluorine F 18 decays by emitting positron to Oxygen O 16 (stable) and has a physical half-life of 109.7 minutes. The principal photons useful for imaging are the dual 511 keV gamma photons, that are produced and emitted simultaneously in opposite direction when the positron interacts with an electron (Table 2).

Table 2. Pricipal Radiation Emission Data for Fluorine F18

Radiation/Emission	% Per Disintegration	Mean Energy
Positron (b+)	96.73	249.8 keV
Gamma (±)*	193.46	511.0 keV

*Produced by positron annihilation

From: Kocher, D.C. Radioactive Decay Tables DOE/TIC-I 1026, 89 (1981)

The specific gamma ray constant (point source air kerma coefficient) for fluorine F 18 is 5.7 R/hr/mCi (1.35 x 10-6 Gy/hr/kBq) at 1 cm. The half-value layer (HVL) for the 511 keV photons is 4 mm lead (Pb). The range of attenuation coefficients for this radionuclide as a function of lead shield thickness is shown in Table 3. For example, the interposition of an 8 mm thickness of Pb, with a coefficient of attenuation of 0.25, will decrease the external radiation by 75%.

Table 3. Radiation Attenuation of 511 keV Photons by lead (Pb) shielding

Shield thickness (Pb) mm	Coefficient of attenuation
0	0.00
4	0.50
8	0.25
13	0.10
26	0.01
39	0.001
52	0.0001

For use in correcting for physical decay of this radionuclide, the fractions remaining at selected intervals after calibration are shown in Table 4.

Table 4. Physical Decay Chart for Fluorine F18

Minutes	Fraction Remaining
0*	1.000
15	0.909
30	0.826
60	0.683
110	0.500
220	0.250

*calibration time

12 CLINICAL PHARMACOLOGY

12.1 Mechanism of Action

Fludeoxyglucose F 18 is a glucose analog that concentrates in cells that rely upon glucose as an energy source, or in cells whose dependence on glucose increases under pathophysiological conditions. Fludeoxyglucose F 18 is transported through the cell membrane by facilitative glucose transporter proteins and is phosphorylated within the cell to [^{18}F] FDG-6-phosphate by the enzyme hexokinase. Once phosphorylated it cannot exit until it is dephosphorylated by glucose-6-phosphatase. Therefore, within a given tissue or pathophysiological process, the retention and clearance of Fludeoxyglucose F 18 reflect a balance involving glucose transporter, hexokinase and glucose-6-phosphatase activities. When allowance is made for the kinetic differences between glucose and Fludeoxyglucose F 18 transport and phosphorylation (expressed as the ‚lumped constant" ratio), Fludeoxyglucose F 18 is used to assess glucose metabolism.

In comparison to background activity of the specific organ or tissue type, regions of decreased or absent uptake of Fludeoxyglucose F 18 reflect the decrease or absence of glucose metabolism. Regions of increased uptake of Fludeoxyglucose F 18 reflect greater than normal rates of glucose metabolism.

12.2 Pharmacodynamics

Fludeoxyglucose F 18 Injection is rapidly distributed to all organs of the body after intravenous administration. After background clearance of Fludeoxyglucose F 18 Injection, optimal PET imaging is generally achieved between 30 to 40 minutes after administration.

In cancer, the cells are generally characterized by enhanced glucose metabolism partially due to (1) an increase in activity of glucose transporters, (2) an increased rate of phosphorylation activity, (3) a reduction of phosphatase activity or, (4) a dynamic alteration in the balance among all these processes. However, glucose metabolism of cancer as reflected by Fludeoxyglucose F 18 accumulation shows considerable variability. Depending on tumor type, stage, and location, Fludeoxyglucose F 18 accumulation may be increased, normal, or decreased. Also, inflammatory cells can have the same variability of uptake of Fludeoxyglucose F 18.

In the heart, under normal aerobic conditions, the myocardium meets the bulk of its energy requirements by oxidizing free fatty acids. Most of the exogenous glucose taken up by the myocyte is converted into glycogen. However, under ischemic conditions, the oxidation of free fatty acids decreases, exogenous glucose becomes the preferred myocardial sub strate, glycolysis is stimulated, and glucose taken up by the myocyte is metabolized immediately instead of being converted into glycogen. Under these condi-

tions, phosphorylated Fludeoxyglucose F 18 accumulates in the myocyte and can be detected with PET imaging.

In the brain, cells normally rely on aerobic metabolism. In epilepsy, the glucose metabolism varies. Generally, during a seizure, glucose metabolism increases. Interictally, the seizure focus tends to be hypometabolic.

12.3 Pharmacokinetics

Distribution: In four healthy male volunteers, receiving an intravenous administration of 30 seconds in duration, the arterial blood level profile for Fludeoxyglucose F 18 decayed triexponentially. The effective half-life ranges of the three phases were 0.2 to 0.3 minutes, 10 to 13 minutes with a mean and standard deviation (STD) of 11.6 (±) 1.1 min, and 80 to 95 minutes with a mean and STD of 88 (±) 4 min.

Plasma protein binding of Fludeoxyglucose F 18 has not been studied.

Metabolism: Fludeoxyglucose F 18 is transported into cells and phosphorylated to [^{18}F]-FDG-6- phosphate at a rate proportional to the rate of glucose utilization within that tissue. [F18]-FDG-6-phosphate presumably is metabolized to 2-deoxy-2-[F18]fluoro-6-phospho-D-mannose([F 18]FDM-6-phosphate).

Fludeoxyglucose F 18 Injection may contain several impurities (e.g., 2-deoxy-2-chloro-D-glucose (ClDG)). Biodistribution and metabolism of ClDG are presumed to be similar to Fludeoxyglucose F 18 and would be expected to result in intracellular formation of 2-deoxy-2-chloro-6-phospho-D-glucose (ClDG-6-phosphate) and 2-deoxy-2-chloro-6-phospho-D-mannose (ClDM-6-phosphate). The phosphorylated deoxyglucose compounds are dephosphorylated and the resulting compounds (FDG, FDM, ClDG, and ClDM) presumably leave cells by passive diffusion. Fludeoxyglucose F 18 and related compounds are cleared from non-cardiac tissues within 3 to 24 hours after administration. Clearance from the cardiac tissue may require more than 96 hours. Fludeoxyglucose F 18 that is not involved in glucose metabolism in any tissue is then excreted in the urine.

Elimination: Fludeoxyglucose F 18 is cleared from most tissues within 24 hours and can be eliminated from the body unchanged in the urine. Three elimination phases have been identified in the reviewed literature. Within 33 minutes, a mean of 3.9% of the administrated radioactive dose was measured in the urine. The amount of radiation exposure of the urinary bladder at two hours post-administration suggests that 20.6% (mean) of the radioactive dose was present in the bladder.

Special Populations:

The pharmacokinetics of Fludeoxyglucose F 18 Injection have not been studied in renally-impaired, hepatically impaired or pediatric patients. Fludeoxyglucose F 18 is eliminated through the renal system. Avoid excessive radiation exposure to this organ system and adjacent tissues.

The effects of fasting, varying blood sugar levels, conditions of glucose intolerance, and diabetes mellitus on Fludeoxyglucose F 18 distribution in humans have not been ascertained [see Warnings and Precautions (5.2)].

13 NONCLINICAL TOXICOLOGY

13.1 Carcinogenesis, Mutagenesis, Impairment of Fertility

Animal studies have not been performed to evaluate the Fludeoxyglucose F 18 Injection carcinogenic potential, mutagenic potential or effects on fertility.

14 CLINICAL STUDIES

14.1 Oncology

The efficacy of Fludeoxyglucose F 18 Injection in positron emission tomography cancer imaging was demonstrated in 16 independent studies. These studies prospectively evaluated the use of Fludeoxyglucose F 18 in patients with suspected or known malignancies, including non-small cell lung cancer, colo-rectal, pancreatic, breast, thyroid, melanoma, Hodgkin's and non-Hodgkin's lymphoma, and various types of metastatic cancers to lung, liver, bone, and axillary nodes. All these studies had at least 50 patients and used pathology as a standard of truth. The Fludeoxyglucose F 18 Injection doses in the studies ranged from 200 MBq to 740 MBq with a median and mean dose of 370 MBq.

In the studies, the diagnostic performance of Fludeoxyglucose F 18 Injection varied with the type of cancer, size of cancer, and other clinical conditions. False negative and false positive scans were observed. Negative Fludeoxyglucose F 18 Injection PET scans do not exclude the diagnosis of cancer. Positive Fludeoxyglucose F 18 Injection PET scans can not replace pathology to establish a diagnosis of cancer. Non-malignant conditions such as fungal infections, inflammatory processes and benign tumors have patterns of increased glucose metabolism that may give rise to false-positive scans. The efficacy of Fludeoxyglucose F 18 Injection PET imaging in cancer screening was not studied.

14.2 Cardiology

The efficacy of Fludeoxyglucose F 18 Injection for cardiac use was demonstrated in ten independent, prospective studies of patients with coronary artery disease and chronic left ventricular systolic dysfunction who were scheduled to undergo coronary revascularization. Before revascularization, patients underwent PET imaging with Fludeoxyglucose F 18 Injection (74 to 370 MBq, 2 to 10 mCi) and perfusion imaging with other diagnostic radiopharmaceuticals. Doses of Fludeoxyglucose F 18 Injection ranged from 74 to 370 MBq (2 to 10 mCi). Segmental, left ventricular, wall-motion assessments of asynergic areas made before revascularization were compared in a blinded manner to assessments made after successful revascularization to identify myocardial segments with functional recovery.

Left ventricular myocardial segments were predicted to have reversible loss of systolic function if they showed Fludeoxyglucose F 18 accumulation and reduced perfusion (i.e., flow-metabolism mismatch). Conversely, myocardial segments were predicted to have irreversible loss of systolic function if they showed reductions in both Fludeoxyglucose F 18 accumulation and perfusion (i.e., matched defects).

Findings of flow-metabolism mismatch in a myocardial segment may suggest that successful revascularization will restore myocardial function in that segment. However, false-positive tests occur regularly, and the decision to have a patient undergo revascularization should not be based on PET findings alone. Similarly, findings of a matched defect in a myocardial segment may suggest that myocardial function will not recover in that segment, even if it is successfully revascularized. However, false-negative tests occur regularly, and the decision to recommend against coronary revascularization, or to recommend a cardiac transplant, should not be based on PET findings alone. The reversibility of segmental dysfunction as predicted with Fludeoxyglucose F 18 PET imaging depends on successful coronary revascularization. Therefore, in patients with a low likelihood of successful revascularization, the diagnostic usefulness of PET imaging with Fludeoxyglucose F 18 Injection is more limited.

14.3 Neurology

In a prospective, open label trial, Fludeoxyglucose F 18 Injection was evaluated in 86 patients with epilepsy. Each patient received a dose of Fludeoxyglucose F 18 Injection in the range of 185 to 370 MBq (5 to 10 mCi). The mean age was 16.4 years (range: 4 months to 58 years; of these, 42 patients were less than 12 years and 16 patients were less than 2 years old). Patients had a known diagnosis of complex partial epilepsy and were under evaluation for surgical treatment of their seizure disorder. Seizure foci had been previously identified on ictal EEGs and sphenoidal EEGs. Fludeoxyglucose F 18 Injection PET imaging confirmed previous diagnostic findings in 16% (14/87) of the patients; in 34% (30/87) of the patients, Fludeoxyglucose F 18 Injection PET images provided new findings. In 32% (27/87), imaging with Fludeoxyglucose F 18 Injection was inconclusive. The impact of these imaging findings on clinical outcomes is not known.

Several other studies comparing imaging with Fludeoxyglucose F 18 Injection results to subsphenoidal EEG, MRI and/or surgical findings supported the concept that the degree of hypometabolism corresponds to areas of confirmed epileptogenic foci. The safety and effectiveness of Fludeoxyglucose F 18 Injection to distinguish idiopathic epileptogenic foci from tumors or other brain lesions that may cause seizures have not been established.

15 REFERENCES

1. Gallagher B.M., Ansari A., Atkins H., Casella V., Christman D.R., Fowler J.S., Ido T., MacGregor R.R., Som P., Wan C.N., Wolf A.P., Kuhl D.E., and Reivich M. "Radiopharmaceuticals XXVII. 18F-labeled 2-deoxy-2-fluoro-d-glucose as a radiopharmaceutical for measuring regional myocardial glucose metabolism in vivo: tissue distribution and imaging studies in animals," J Nucl Med, 1977; 18, 990-6.
2. Jones S.C., Alavi, A., Christman D., Montanez, I., Wolf, A.P., and Reivich M. "The radiation dosimetry of 2 [F-18] fluoro-2-deoxy-D-glucose in man," J Nucl Med, 1982; 23, 613-617.
3. Kocher, D.C. "Radioactive Decay Tables: A handbook of decay data for application to radiation dosimetry and radiological assessments," 1981, DOE/TIC-I 1026, 89.
4. ICRP Publication 53, Volume 18, No. I-4,1987, pages 75-76.

16 HOW SUPPLIED/STORAGE AND DRUG HANDLING

Fludeoxyglucose F 18 Injection is supplied in a multi-dose, capped 30 mL and 50 mL glass vial containing between 0.740 to 7.40 GBq/mL (20 to 200 mCi/mL), of no carrier added 2-deoxy-2-[F 18] fluoro-D-glucose, at end of synthesis, in approximately 15 to 50 mL. The contents of each vial are sterile, pyrogen-free and preservative-free.

NDC 40028-511-30; 40028-511-50

Receipt, transfer, handling, possession, or use of this product is subject to the radioactive material regulations and licensing requirements of the U.S. Nuclear Regulatory Commission, Agreement States or Licensing States as appropriate.

Store the Fludeoxyglucose F 18 Injection vial upright in a lead shielded container at 25°C (77°F); excursions permitted to 15-30°C (59-86°F).

Store and dispose of Fludeoxyglucose F 18 Injection in accordance with the regulations and a general license, or its equivalent, of an Agreement State or a Licensing State.

The expiration date and time are provided on the container label. Use Fludeoxyglucose F 18 Injection within 12 hours from the EOS time.

17 PATIENT COUNSELING INFORMATION

Instruct patients in procedures that increase renal clearance of radioactivity. Encourage patients to:

- drink water or other fluids (as tolerated) in the 4 hours before their PET study.
- void as soon as the imaging study is completed and as often as possible thereafter for at least one hour.

Manufactured by: PETNET Solutions Inc.
810 Innovation Drive
Knoxville, TN 37932

Distributed by: PETNET Solutions Inc.
810 Innovation Drive
Knoxville, TN 37932

PETNET Solutions

PN0002262 Rev. A
March 1, 2011

On account of certain regional limitations of sales rights and service availability, we cannot guarantee that all products included in this brochure are available through the Siemens sales organization worldwide. Availability and packaging may vary by country and is subject to change without prior notice. Some/All of the features and products described herein may not be available in the United States.

The information in this document contains general technical descriptions of specifications and options as well as standard and optional features which do not always have to be present in individual cases.

Siemens reserves the right to modify the design, packaging, specifications and options described herein without prior notice.

Please contact your local Siemens sales representative for the most current information.

Note: Any technical data contained in this document may vary within defined tolerances. Original images always lose a certain amount of detail when reproduced.

Local Contact Information

Asia/Pacific:
Siemens Medical Solutions
Asia Pacific Headquarters
The Siemens Center
60 MacPherson Road
Singapore 348615
Phone: +65 9622-2026
www.siemens.com/healthcare

Canada:
Siemens Canada Limited
Medical Solutions
2185 Derry Road West
Mississauga ON L5N 7A6
Canada
Phone: +1 905 819-5800
www.siemens.com/healthcare

Europe/Africa/Middle East:
Siemens AG
Medical Solutions
Henkestraße 127
D-91052 Erlangen
Germany
Phone: +49 9131 84-0
www.siemens.com/healthcare

Latin America:
Siemens S.A.
Medical Solutions
Avenida de Pte. Julio A. Roca No 516, Piso 7
C1067ABN Buenos Aires Argentina
Phone: +54 11 4340-8400
www.siemens.com/healthcare

USA:
Siemens Medical Solutions USA, Inc.
51 Valley Stream Parkway
Malvern, PA 19355-1406
USA
Phone: +1-888-826-9702
www.siemens.com/healthcare

Global Siemens Headquarters

Siemens AG
Wittelsbacherplatz 2
80333 Muenchen
Germany

Global Siemens Healthcare Headquarters

Siemens AG
Healthcare Sector
Henkestraße 127
91052 Erlangen
Germany
Phone: +49 9131 84-0
www.siemens.com/healthcare

Order No. A91MI-10423-1T-7600 | Printed in USA | MI-2213.RM.JV.TW.1500

www.siemens.com/imaginglife